NASA Technical Memorandum 78666

(NASA-TM-78666) ONSET OF CONDENSATION EFFECTS WITH A NACA 0012-64 AIRFOIL TESTED IN THE LANGLEY 0.3-METER CRYOGENIC TUNNEL (NASA) 84 p HC A05/MF A01 CSCL 01A

N78-20074

Unclas

G3/02 11898

ONSET OF CONDENSATION EFFECTS WITH A NACA 0012-64 AIRFOIL TESTED IN THE LANGLEY 0.3-METER CRYOGENIC TUNNEL

Robert M. Hall

March 1978

National Aeronautics and Space Administration

Langley Research Center
Hampton, Virginia 23665

SUMMARY

A 0.137-m NACA 0012-64 airfoil has been tested in the Langley 0.3-m transonic cryogenic tunnel at free-stream Mach numbers of 0.75, 0.85, and 0.95 over a total pressure range from 1.2 to 5.0 atmospheres. The onset of condensation effects were found to correlate more with the amount of supercooling in the free-stream than it did with the supercooling in the region of maximum local Mach number over the airfoil. Effects in the pressure distribution over the airfoil were generally seen to appear over its entire length at nearly the same total temperature. Both observations suggest the possibility of heterogeneous nucleation occurring in the free-stream. Comparisons of the present onset results are made to calculations by Sivier and data by Goglia. The potential operational benefits of the supercooling realized are presented in terms of increased Reynolds number capability at a given tunnel total pressure, reduced drive fan power if Reynolds number is held constant, and reduced liquid nitrogen consumption if Reynolds number is again constant. Depending on total pressure and free-stream Mach number, these three benefits are found to respectively vary from 7 to 19%, 11 to 25%, and 9 to 20%. Appendices are included which give details of the data analysis procedure and of the error bar calculation for the differences in pressure distributions.

INTRODUCTION

Cryogenic wind tunnels should be operated at the lowest possible total temperatures in order to maximize the advantages of cryogenic operation, such as increased Reynolds number and reduced operating costs. However, minimum operating temperatures are limited by low temperature effects on the flow, which can be the result of real-gas behavior of the test-gas. Either the equation of state of the test-gas changes in such a manner that the gas does not properly simulate the nearly ideal-gas behavior of air encountered in flight, or the gas begins to condense and consequently does not properly simulate the nearly ideal-gas behavior of air. Analyzing the nitrogen test-gas over the operating ranges of existing and proposed transonic cryogenic wind tunnels, Adcock reported in reference 1 that low temperature nitrogen gas approximates an ideal-gas during flow simulations for total pressures under 10 atmospheres and for Mach numbers up to 2. Consequently, the lower temperature boundary appears to be determined by condensation of the nitrogen test-gas. The boundary is important from an operational viewpoint because it determines, on one hand, the maximum Reynolds number capability for a fixed tunnel total pressure and, on the other hand, the most economical total temperature and pressure to operate the tunnel for a fixed test Reynolds number.

Condensation not only has an important role in determining the operational envelope for transonic cryogenic tunnels but has a similar role for supersonic and hypersonic tunnels. Wegener and Mack in reference 2 give a summary of historical events leading to, and the results from, many of the condensation investigations in supersonic and hypersonic tunnels.

The present condensation investigation employs a pressure-instrumented NACA 0012-64 airfoil mounted in the Langley 0.3-m transonic cryogenic tunnel. Changes in the pressure distribution over the airfoil have been used to detect the onset of condensation effects in a similar fashion as changes in pressure distributions in divergent nozzles were used in references 2 to 6 to detect the onset of condensation effects at supersonic and hypersonic speeds. The airfoil has been tested at free-stream Mach numbers of 0.75, 0.85, and 0.95 over a total pressure range of 1.2 to 5.0 atmospheres in order to determine the total temperature at which condensation influences the flow about the airfoil as a function of total pressure and free-stream Mach number.

SYMBOLS

a	sound speed
c	airfoil chord, 0.137-m
C_p	pressure coefficient, $\frac{p - p_\infty}{q_\infty}$
ΔC_p	difference in C_p defined by equation (A6)
p	pressure, atm
Δp	pressure instrumentation accuracy
q	dynamic pressure
R	Reynolds number
T	temperature, K
ΔT	supercooling defined by equation (1)
x	linear dimension along airfoil chord line
μ	viscosity
ρ	density
σ	standard deviation

Subscripts

e	conditions at onset of condensation effects
L	local conditions
s	conditions at intersection of isentrope and vapor pressure curve
t	total conditions
∞	free-stream conditions

MINIMUM OPERATING TEMPERATURES

The maximum Reynolds number capability and the operating costs of a cryogenic wind tunnel are both affected by the minimum operating temperatures of the tunnel. The reasons for this can be understood by reviewing the effects of changing tunnel temperature upon the test gas, which are shown in figures 1(a) and 1(b). In figure 1(a) the behavior of the gas properties relative to their ambient temperature values can be seen. The density, ρ, increases while the viscosity, μ, and the speed of sound, a, decrease as the total temperature, T_t, decreases for a fixed value of tunnel total pressure, p_t. As shown in figure 1(b), the behavior of the gas properties as T_t decreases leads to a dramatic increase in unit Reynolds number, R, a decrease in drive power required, and no change in dynamic pressure, q. Consequently, it is desirable to operate the tunnel as cold as is possible in order to maximize R and reduce drive power. Just how low in temperature the tunnel can be operated is determined by the onset of condensation effects.

A conservative first guess for the minimum operating temperature is to operate at temperatures which avoid any possibility of saturation occurring anywhere over the model. Since the lowest static temperature over a model occurs at the point of maximum local Mach number, $M_{L_{max}}$, T_t and p_t can be chosen to keep the local static values of p, T just on the vapor phase side of the vapor pressure curve for nitrogen. However, it has been found from tests in the Langley 0.3-m transonic cryogenic tunnel and in other facilities that condensation effects tend to be delayed to some lower temperature.

The delay in condensation onset past the vapor-pressure curve is due to an energy barrier blocking stable liquid droplet formation - that is, blocking self-nucleation of the test gas. Thus there will normally be a delay in droplet formation and growth, and consequently in effects, unless some catalyst is available to speed the process. (More details of the various condensation processes will be given in the section Implications of the Data.) The delay in condensation can be quantitatively measured by the supercooling at onset of effects, ΔT, which is defined as

$$\Delta T = T_s - T_e \tag{1}$$

where T_s is the static temperature where the isentrope crosses the vapor pressure curve and T_e is the static temperature along the isentrope where effects are first seen.

If supercooling does occur then there are two wind tunnel operational benefits that result. First of all, for a given tunnel p_t the maximum R capability is increased because at the lower temperature the unit R is greater as shown in figure 1(b). This benefit would not only increase the maximum R capability of a tunnel, but would also increase the R obtainable for a model that may be q limited since q is proportional to p_t for a given M_∞. Secondly, if maximum R capability is not important, then supercooling can be used to reduce operating costs when operating at a fixed R. Operating at a lower T_t than needed to avoid saturation permits a decrease in p_t for a given value of R. Since drive fan power is proportional to p_t and decreases with decreasing T_t, both changes reduce the required drive power. Since normally over 99% of the injected liquid nitrogen is used to absorb the heat generated by the drive fan once the tunnel has been cooled, a reduction in drive fan power leads to a reduction in the amount of injected liquid nitrogen.

Both reductions decrease direct operating costs, which are split with about 90% going to the injected liquid nitrogen and only 10% going to power the drive fan. Specific details of drive power required and operating costs are given in references 7 and 8.

EXPERIMENTAL APPARATUS

Tunnel

The Langley 0.3-m transonic cryogenic tunnel is a continuous flow, fan-driven tunnel, which uses nitrogen as a test gas and is cooled by injecting liquid nitrogen directly into the stream. Variation of the rate of liquid nitrogen injection provides a total temperature range from nearly 77 to 350 K, while the total pressure can be varied from 1.2 to 5.0 atm. The combined low temperature and high pressure can produce a Reynolds number of over 330 million/m (100 million/ft). Some of the design features and operational characteristics of the 0.3-m tunnel have been reported by Kilgore in reference 9, and a sketch of the tunnel is shown in figure 2.

The liquid nitrogen used to cool down the tunnel and absorb the heat of the drive fan was injected into the tunnel through a series of eleven nozzles arranged on three different struts, or spray bars, at the three injection stations shown in figure 2. Full details of this arrangement are included in reference 9. However, for one of the tests during the present investigation (details to be mentioned in RESULTS AND DISCUSSION), the spray bar system was removed and injection was carried out by injecting through just four nozzles at injection station 1. This change, of course, necessitated larger liquid flow rates per nozzle.

Airfoil and Installation

A 0.137-m NACA 0012-64 airfoil was used for these tests. Starting at the leading edge, the airfoil had 20 pressure orifices spaced at 5% chord intervals on both the top and bottom surfaces. For the tests at M_∞ of 0.75 and 0.95, a rearward-facing orifice was added to the trailing edge of the airfoil. The airfoil was installed between flats in the octagonal test section, with the leading edge 0.62-m from the beginning of the test section. The angle of attack of the airfoil was zero for all tests. A sketch of the airfoil is given in figure 3.

The pressure distributions over the airfoil may be influenced by wall interference effects because of the relatively large chord of the airfoil compared to the size of the test section. However, wall interference should not have an effect on the occurrence of condensation.

Data Acquisition and Error Discussion

The tunnel parameters were first recorded and then a differential pressure transducer was used in a scanning valve system to step through and record the pressures around the airfoil. The time to acquire all of the data for a complete pressure distribution was 50 seconds.

The uncertainty in the pressure transducer measurements was less than 0.5 percent of full scale, which was the magnitude specified by the manufacturer. In fact, the scatte in the pressure transducer data was observed to be less than the stated value by more than a factor of 10. For the transducer used in the tests at $M_\infty = 0.75$ and 0.95, the uncertainty was on the order of 0.0004 atm. For the transducer used in the test at $M_\infty = 0.85$, the uncertainty was about 0.0002 atm. There was no significant error introduced by either the signal conditioning or data acquisition systems. However, during the 50-second acquisition period, the tunnel conditions were observed to fluctuate by the following amounts: M_∞, ±.003; T_t, ±0.5K; and p_t, approximately ±0.005 atm. A development of the uncertainty in C_p due to the above fluctuations is contained in appendix B.

TESTS

Data Sampled

To determine the total temperature at which effects do occur and to investigate the influence of total pressure and free-stream Mach number on the onset of condensation effects, the airfoil was tested at free-stream Mach numbers of 0.75, 0.85, and 0.95 over a total pressure range of 1.2 to 5.0 atm. For each of the three values of M_∞, test envelopes were drawn which covered those tunnel p_t and T_t ranges that were of interest and that were obtainable in the 0.3-m tunnel.

The test envelopes were bounded in p_t by the 1.2 to 5.0 atm pressure limits of the tunnel and were bounded in T_t by total temperatures corresponding to saturated flow at $M_{L_{max}}$ and those corresponding to saturation in the reservoir section. Figure 4 shows the $M_\infty = 0.85$ test envelope as an example. Total conditions which fall lower in T_t than the reservoir saturation line are unobtainable since the injected liquid nitrogen used for cooling would never evaporate when T_t is below the vapor pressure curve and, consequently, furth cooling can not occur. Total temperatures above those along the line of local saturation offer no possibility of condensation in a pure nitrogen test-gas so they are used in this study only as a way of obtaining unaffected comparison points. The locus of tunnel p_t and T_t which just allow saturation when the flow is accelerated to M_∞ is also given in figure 4.

To explore each of the regions of interest in the p_t and T_t plane, paths of constant R_c and M_∞ were used to traverse the region of interest. Since along each of the paths both M_∞ and R_c were held constant, systematic deviation in pressure coefficients at any x/c position over the airfoil was taken to be the result of condensation effects. The paths of constant R_c and M_∞ are shown for the $M_\infty = 0.85$ test in figure 5. The R_c along each path varied from 16 million at the low pressure traverse to 42 million at the high pressure traverse. Along these 5 paths, a total of 201 pressure distributions were recorded and analyzed. Similar envelopes were drawn and investigated for $M_\infty = 0.75$ and $M_\infty = 0.95$ except that only 3 paths of constant R_c and M_∞ were used in these cases. These envelopes are shown in figures 6 and 7. During the investigation of the high pressure path for the $M_\infty = 0.95$ test, a fan drive power limit was encountered so M_∞ was reduced from 0.95 to 0.93 for that path alone.

Data Analysis

In order to determine the p_t and T_t at which the onset of condensation effects occurs along a constant M_∞ and R_c path, a special data analysis procedure was developed. The main objective of the data analysis procedure was to be able to correct values of C_p on an orifice-by-orifice basis in cases where the pressure distribution over the airfoil was taken at a slightly different M_∞ than desired. With such a correction, data along the path that normally would have had to be disregarded due to small differences in M_∞ could be utilized. Having more data available made it easier to detect the total temperature at which differences in C_p, ΔC_p, begin to occur because of the effects of condensation.

Once the values of total temperature for the onset of effects at each orifice had been determined, a graph of orifice onset total temperature as a function of x/c could be drawn for the path of constant M_∞ and R_c. In this manner, an appropriate onset total temperature could be chosen for the airfoil as a whole. Further details of the data analysis procedure are presented in appendix A.

RESULTS AND DISCUSSION

Data Presentation and Comments

The data, taken and analyzed as discussed in the previous section, will be summarized by a series of figures for each value of M_∞ - 0.75, 0.85, and 0.95 - covered in this study. Each series will include average, condensation-free pressure distributions for each path of constant R_c; graphs of orifice onset T_t as a function of x/c for each path; and a summary plot for each M_∞ showing the onset conditions for each path in a T_t versus p_t plane. The results for all of the M_∞ will then be grouped together assuming either $M_{L_{max}}$ or M_∞ is the important Mach number parameter.

The first test described is the $M_\infty = 0.75$ test. The average pressure distributions are shown in figures 8, 9, and 10, and the orifice onset T_t vs. x/c graphs are shown in figures 11, 12, and 13. Four different symbols are plotted in the orifice onset graphs corresponding to four different situations. When normal orifice onset is detected, a circle is plotted at the appropriate x/c, T_t location. When no orifice onset is detected, a square is plotted at the minimum T_t at which data was taken. When excessive scatter obscures any trends, a triangle is plotted at the minimum T_t. When an orifice pressure tube developed a leak, a diamond is plotted at the minimum T_t. It is interesting to note in figures 11, 12, and 13 that the airfoil appears to be most sensitive to condensation effects in the 15-25% chord location, as is seen most clearly in figures 12 and 13. There does not seem to be any greater sensitivity to condensation over the rearward portion of the airfoil, which seems to downplay the importance of any condensate growth over the airfoil itself. The summary plot of onset conditions is shown in figure 14.

The pressure distributions for the 5 lines of constant R_c for the $M_\infty = 0.85$ test are shown in figures 15, 16, 17, 18, and 19 and exhibit a recompression shock at the 0.65 x/c location. The graphs showing orifice onset T_t as a function of x/c are shown in figures 20, 21, 22, 23, and 24. With the possible exception of figure 24, it appears that effects occur at about the same T_t over the length of the airfoil. That is, there is not an obvious sensitivity to condensation effects behind the shock, or even right before the shock in the region of high local Mach number. Along the $R_c = 42$ million path as shown in figure 24, there does appear to be possible sensitivity behind the shock location. At x/c values of 0.75 and 0.85 the onset value of T_t appeared to be 100.5 K, which is above the trend of effects occurring at about 96 or 96.5 K for the majority of orifices. While the onset T_t of 100.5 K may be correct, there is scatter in the ΔC_p vs. T_t graphs that were combined to form figure 24. Because of the uncertainties involved and because of the lack of agreement between orifice onset T_t's behind the shock location at x/c = 0.65 in figure 24, the airfoil onset T_t was chosen to be 98.5 K with a possible error bar extending from 96.5 to 100.5 K. The summary plot of onset conditions for the $M_\infty = 0.85$ test is given in figure 25.

The last test condition was that of $M_\infty = 0.95$. As mentioned under the section Data Sampled, the high pressure path at $R_c = 40$ million was tested at $M_\infty = 0.93$ instead of 0.95, so there is a M_∞ difference between the first 2 paths and the $R_c = 40$ million path. The unaffected pressure distributions are shown in figures 26, 27, and 28, and the orifice onset T_t vs. x/c graphs are presented in figures 29, 30, and 31. The onset T_t's for the $R_c = 16$ million path do not seem to have any one area more sensitive than any others, as seen in figure 29. However, onset T_t's for the R_c = 27 million path in figure 30 may be showing signs of an increased sensitivity at about $x/c = 0.40$ in the region of increasing local Mach number, although the trend is not conclusive. The third path at R_c = 40 million shows a very uniform onset T_t over the airfoil. There was no data taken along this path between $T_t = 100.5$ and $T_t = 103.5$; consequently, there is no resolution of effects between these 2 temperatures and this may contribute to the fairly uniform distribution of onset T_t. The lack of resolution is indeed unfortunate as seen in figure 32, which shows ΔC_p vs. T_t for $x/c = 0.95$, because there are no effects at $T_t = 103.5$ K but well developed effects at 100.5 K. For this path, onset T_t for the airfoil was chosen to be 102.0 K with the error bar spanning 100.5 to 103.5 K. The summary plot for onset conditions for the $M_\infty = 0.95$ test is given in figure 33.

The results for all of the M_∞ tests will now be grouped together assuming first that $M_{L_{max}}$ is the important Mach number parameter and then assuming that M_∞ is the important parameter. The question of which Mach number is important arises because of the uncertainty in the mode of nucleation that is occurring, which is discussed in the next section.

The first pair of figures comparing all of the onset results is constructed for the supercooling as defined in equation (1).

$$\Delta T = T_s - T_e \qquad (1)$$

In equation (1), the value of T_s is the static temperature at which the isentrope, starting at the onset values of p_t and T_t, crosses the vapor-pressure curve. The value of T_e is the static temperature along the same isentrope at $M = M_{L_{max}}$ in figure 34(a) and at $M = M_\infty$ in figure 34(b).

In both cases the value of ΔT is plotted as a function of the onset P_t along each path of constant R_c. In figure 34(a), the supercooling was nearly constant at 7 K over the pressure range for $M_\infty = 0.75$, was roughly equal to 11 K over the pressure range for $M_\infty = 0.85$, and was 12 and 14 K for the two lower pressure paths at $M_\infty = 0.95$ and then dropped to 10 K for the high pressure path. In figure 34(b), the supercooling based on M_∞ remained between 2 and 3 K over the pressure range for both $M_\infty = 0.75$ and 0.85. However, the supercooling for the $M_\infty = 0.95$ test was 1 and 2 K for the lower pressure paths, but dropped to -2 K for the upper pressure path. Regardless of the behavior of the high pressure path for the $M_\infty = 0.95$ test, there seems to be much better correlation of the values for supercooling when assuming M_∞ is the pertinent Mach number rather than $M_{L_{max}}$.

The second pair of figures again compares all of the onset results, but the comparison is now made in a $\log_{10} p$ versus T plane. Static values of p, T are calculated from the p_t and T_t at onset and are calculated assuming an isentropic expansion to either $M_{L_{max}}$ or M_∞. Figure 35(a) shows the p, T as calculated assuming $M_{L_{max}}$ is the Mach number of interest while figure 35(b) shows the p, T as calculated assuming M_∞ is the important Mach number. It would again appear from figure 35, as in figure 34, that the onset data correlates much better with M_∞ than with $M_{L_{max}}$.

The seemingly early onset of effects in the high pressure path of the $M_\infty = 0.95$ test may be the result of a tunnel configuration change that was made before the data for this path was taken. The spray bars system used for injection of the liquid nitrogen as described under the tunnel apparatus was removed for another investigation in the .3-m tunnel and remained out for the tunnel entry during which the data was obtained for the high pressure path of the $M_\infty = 0.95$ test. With the spray bars removed the liquid was injected from four nozzles flush with the interior tunnel wall at injection station 1 instead of the eleven nozzles at the three different stations. Consequently, the liquid injected may not have broken up and evaporated as effectively as it did with the eleven nozzles. The unevaporated drops may have formed the increased number of nucleating sites necessary to decrease the amount of supercooling realized. Because of this uncertainty due to the tunnel configuration change, the data from the high pressure path of the $M_\infty = 0.95$ test will not be presented in further data comparison graphs.

Implications of the Data

Condensation effects can be caused by three different modes of nucleation, where nucleation is taken as the formation of a stable liquid droplet. The three different modes are homogeneous, heterogeneous, and binary nucleation. These three processes differ by the manner in which they overcome an energy barrier to droplet formation and hence growth. In depth discussion of the three types can be found in references 2, 3, 4, 10, 11, 12, and 13. The different modes can briefly be summarized as follows.

Homogeneous nucleation can occur when the gas undergoes supercooling, which will decrease the energy barrier to liquid droplet formation. When enough supercooling occurs, the gas molecules will be able to overcome the energy barrier to droplet formation and massive nucleation rates are likely. Heterogeneous nucleation may occur when there are liquid or solid impurities suspended in the vapor at the time the flow first expands past the vapor-pressure curve and begins to supercool. The energy barrier of formation, which is so important for homogeneous condensation, is not so significant here because the impurities can act as a catalyst for the condensation process.

Consequently, little or no supercooling is needed before stable droplet growth occurs. What prevents heterogeneous nucleation from always dominating the homogeneous process is that it requires extremely large concentrations of impurity sites to influence the flow as was pointed out by Wegener and Mack in reference 2. The third type of nucleation possible is binary. This process occurs when a mixture of two different gases condenses into droplets which are composed of both types of molecules. The binary process is discussed specifically in references 10 to 13. The combination of the two species can effectively change the energy barrier to nucleation in such a manner that condensation will occur earlier than analysis would predict for either of the species acting singly.

The data from the present experiment does seem to suggest which nucleation process might have occurred. First, no condensation seems to be occurring until at least 7 K of supercooling has taken place at the $M_{L_{max}}$ location. If binary nucleation is occurring with some sort of impurity vapor in the nitrogen used for cooling the tunnel, then its effects were either undetectable or occurred at low enough temperature to be confused with homogeneous or heterogeneous nucleation of the nitrogen test gas. The purity of the liquid nitrogen injected for cooling was approximately 99.95 percent in the present experiments, so it is assumed that binary nucleation would be unlikely. Second, none of the orifice onset T_t versus x/c plots show any systematic trend toward condensation first appearing in the region of maximum supercooling, which is the region of high local Mach number. Since the amount of supercooling is so important for homogeneous nucleation, these results do not seem consistent with what one would expect if homogeneous nucleation was occurring. In fact, there seems to be no generally preferred location over the airfoil for effects to occur. Hence the effects may actually be the result of heterogeneous nucleation occurring upstream of the model in the test section. Under these circumstances the airfoil would experience the influence of these droplets over its length at about the same T_t although local sensitivity to the condensate in the free-stream may vary over the airfoil because of differences in M_L or pressure gradient. If condensate in the free-stream is the cause of the effects, the possible source for the impurity sites could be the injected liquid nitrogen used for cooling the tunnel. At the very low temperatures of these tests, the injected liquid may not be completely evaporating in the time it takes to travel from the injection stations to the test section (see figure 2). The partially evaporated droplets may provide the high concentration of nucleation sites needed for heterogeneous condensation. Some evidence for heterogeneous nucleation from unevaporated droplets in the free-stream comes from figures 34 and 35, which show stronger correlation between the onset of effects and M_∞ than the onset of effects and $M_{L_{max}}$. Further evidence comes from the smaller amount of supercooling realized with the high pressure path of the $M_\infty = 0.95$ path. Because the configuration without spray bars is less efficient at breaking up the injected liquid nitrogen, it would seem that the smaller amount of supercooling was due to an increased number of liquid drops on which condensation growth could occur. Light scattering tests should be made in the test-section to determine conclusively if indeed there are unevaporated injection droplets.

Comparison to Other Works

While it appears that heterogeneous nucleation is the cause of condensation in the present experiments, most of the previous condensation investigations have concentrated on homogeneous nucleation. Some of these investigations were concerned with nitrogen gas, and two references, 14 and 15, will be used here for comparison to the present data. A traditional means of presenting onset of effects data is in the $\log_{10} p$ vs. T plane. As mentioned in the previous section, there is some question as to the process of nucleation and hence in the relevant condition to plot in the $\log_{10} p$ vs. T plane. For the present comparisons, it was decided to use the static values of p and T as calculated for the $M_{L_{max}}$ condition because regardless of the source of the effects, this amount of supercooling was realized in the region of maximum local Mach number before effects were detected.

Using the $\log_{10} p$ vs. T format, the present results can be compared with the analytical nitrogen-gas work done by Sivier in reference 14. His computer computations assumed homogeneous nucleation and used classical liquid droplet theory. An unpublished curve fit by Adcock to Sivier's calculated onset points for conditions of higher pressure and lower onset Mach number has been plotted along with the present onset conditions in figure 36, where Adcock's curve fit is represented by

$$\frac{1}{T_e} = 1.461 \times 10^{-2} - 4.962 \times 10^{-3} \times \log_{10} p + 1.959 \times 10^{-4} \times (\log_{10} p)^2 \qquad (2)$$

There is good agreement in trends between the curve fit to Sivier's prediction and the present results although the present onset points fall closer to the vapor-pressure curve than predicted. If Sivier's calculations are accurate, the results would imply that effects are occurring earlier than predicted for homogeneous nucleation. Again, heterogeneous nucleation would be consistent with the data. However, many of the $M_\infty = 0.85$ and 0.95 onset points do approach Sivier's onset line for homogeneous nucleation. If heterogeneous nucleation is indeed occurring then significantly more supercooling may not be possible for the $M_\infty = 0.85$ and 0.95 tests even if the impurity sites were eliminated and homogeneous nucleation took place.

The present results can also be compared to previous experimental results. Goglia in reference 15 has taken data that shows nitrogen onset in the same static pressure and temperature range as considered in the present study. When Goglia's data and the present experimental data are plotted together, as in figure 37, the agreement is especially good considering the fact that the present data consisted of subsonic and supersonic onset points over a 0.137-m airfoil and Goglia's work consisted of rapid expansions in a 0.114-m long nozzle ar onset at Mach numbers from 2.0 to 3.25. Although one would normally expect more supercooling with the larger velocity gradients in the nozzle, it does not show up in the data comparison. In fact, the trend of Goglia's data falls close to the present $M_\infty = 0.75$ data but seems to have somewhat less supercooling than was experienced during the present $M_\infty = 0.85$ or 0.95 data. Goglia states in his conclusion that the condensation he detected appeared to be the result of the self-nucleation, or homogeneous condensation, of the nitrogen test gas. However, the gas used by Goglia was only 95 percent pure nitrogen and contained a 5 percent impurity of oxygen. Even though this fact was well recognized and investigated by Goglia, there may be some effects of heterogeneous nucleation on his onset points. (Arthur and Nagamatsu in reference 6 detected a mild decrease in supercooling of about 1 to 2 K for a 5 percent oxygen impurity.)

Whether or not the condensation in the present investigation was the result of heterogeneous or homogeneous nucleation, it appears that the magnitude of the supercooling is comparable to what others have seen or predicted in the same pressure range.

Benefits Realized

One of the primary motivations for the present experiments was to determine the increase in Reynolds number capability that might be possible when testing an airfoil with supercooled flow. This increase was determined for the NACA 0012-64 airfoil and figure 38 shows the percent increase realized at the temperature at which condensation effects were first detected. The percent increase was calculated by (1) dividing R_c corresponding to p_t and T_t at onset by R_c corresponding to p_t at onset but with T_t being that which just allows local saturation, (2) subtracting one from the resulting ratio, and (3) multiplying by one hundred. As can be seen in figure 38, the $M_\infty = 0.75$ test realized the smallest percent gain in capability at 7%, while the $M_\infty = 0.95$ test realized the largest at 19%. The $M_\infty = 0.75$ and 0.85 tests appear to show a decrease in gain with increasing p_t, while a trend for the $M_\infty = 0.95$ test cannot easily be predicted because of the lack of a high pressure path data point. Error bars shown are calculated from the uncertainty in the value of T_t for the onset of condensation effects over the airfoil.

The second motivation for the present experiment was to determine percent decreases in drive fan power required and in the amount of liquid nitrogen (LN2) injected when unit Reynolds number is held constant and the supercooling is utilized to decrease both p_t and T_t. Since the energy required for producing the amount of LN2 injected is much greater than the energy used by the drive fan, reductions in direct operating costs while at test conditions will be much closer to the percent decrease in LN2 required than to the decrease in drive fan power required.

The decrease in drive fan power realized is shown in figure 39. The trends are, of course, similar to the increase in Reynolds number capability shown in figure 38. For $M_\infty = 0.85$ the decrease in drive power required varied from 21% at low pressure to about 19% at the high pressure end. Decreases of 23 and 25% were found for the two low pressure paths in the $M_\infty = 0.95$ test.

The decrease in LN2 required to absorb drive fan heat is shown in figure 40. For an insulated tunnel such as the Langley 0.3-m tunnel, the injected LN2 required to absorb the heat flow into the tunnel through the tunnel shell insulation is relatively constant over the temperature range of the present tests and is only on the order of 1 percent or less of the amount required to absorb the heat of the drive fan. Consequently, heat leakage through the shell has no effect on figure 40 and has not been included. For the $M_\infty = 0.75$ test, the reduction in LN2 required varied from 11% down to 9% at the higher pressures. For $M_\infty = 0.85$, the reduction varied from 17% at the lower pressures to 15% at the higher pressures. The $M_\infty = 0.95$ test had a reduction high of 20% and a low of 18%.

CONCLUDING REMARKS

An experimental program was undertaken to determine the onset of condensation effects in the pressure distribution about a 0.137-m NACA 0012-64 airfoil tested in the Langley 0.3-m transonic cryogenic tunnel at free-stream Mach numbers of 0.75, 0.85, and 0.95 over a total pressure range from 1.2 to 5.0 atmospheres. Orifice pressure measurements were recorded at 5% chord intervals and were analyzed to determine the total temperature at which deviations first occurred in the orifice pressure coefficient.

The onset of condensation effects were found to correlate more with the amount of supercooling in the free-stream than with the supercooling in the region of maximum local Mach number over the airfoil. Effects in the pressure distribution over the airfoil were generally seen to appear over its entire length at nearly the same total temperature. Both observations suggest the possibility of heterogeneous nucleation occurring in the free-stream. Comparisons of the present onset results are made to calculations by Sivier and data by Goglia.

The potential operational benefits of the supercooling realized were analyzed in terms of increased Reynolds number capability at a given tunnel total pressure, reduced drive fan power if Reynolds number is held constant, and reduced liquid nitrogen consumption if Reynolds number is again constant. Depending on total pressure and free-stream Mach number, these three benefits are found to respectively vary from 7 to 19%, 11 to 25%, and 9 to 20%. Since operating costs at typical test conditions are approximately 10% due to fan drive power and 90% due to liquid nitrogen injection, reduction in operating costs will be very close to the percentage reduction in liquid nitrogen consumption.

Although the present experimental data form a preliminary basis for predicting minimum operating temperatures for nitrogen-gas wind tunnels, it is just one of several steps that are needed for a more complete understanding of the problem. More work is needed in the following areas: tests of other airfoil pressure distributions to determine the sensitivity of the onset of condensation effects to different local velocities and gradients, experiments designed to determine conclusively if condensation is caused by homogeneous or heterogeneous nucleation, studies to determine scaling effects so that the present results may be extended to other sizes of tunnels, and studies to extend the results to higher total pressures.

APPENDIX A

DATA ANALYSIS PROCEDURE

Because of the importance of the data reduction technique upon the detection of the onset of condensation effects, this appendix is included in order to describe in detail the M_∞ correction procedure and to explain the procedure for determining airfoil onset T_t. Examples of the various steps are included for the $M_\infty = 0.85$ and $R_c = 16$ million path.

The M_∞ correction procedure was employed in order to take out as much Mach number effects as possible when comparing C_p's along a path of constant M_∞ and R_c. While M_∞ was nominally constant along a path, many pressure distributions were recorded at values of M_∞ that varied from the nominal value by ±.010. To determine if a M_∞ dependence did exist at a given x/c location, a linear regression technique was applied to condensation-free values of C_p plotted as a function of M_∞. In this manner, if there was a correlation between C_p and M_∞, all of the data could be corrected to a single value of M_∞. If there was little correlation between C_p and M_∞, then a weak dependence was assumed to exist and no correction was assumed necessary. Thus all the data along a given path of constant M_∞ and R_c could be utilized.

The first step of the M_∞ correction procedure is to apply a linear regression technique to values of C_p at a given x/c as a function of M_∞. Using standard definitions as found for example in reference 16, the slope of the linear regression fit would be given by

$$m = \frac{\sum_{i=1}^{n} (M_{\infty_i} - \bar{M}_\infty)(C_{p_i} - \bar{C}_p)}{\sum_{i=1}^{n} (M_{\infty_i} - \bar{M}_\infty)^2} \qquad \text{(A1)}$$

where

$$\bar{M}_\infty = \frac{\sum_{i=1}^{n} M_{\infty_i}}{n} \qquad \text{(A2)}$$

and

$$\bar{C}_p = \frac{\sum_{i=1}^{n} C_{p_i}}{n} \qquad \text{(A3)}$$

The correlation coefficient, r, which is an indication of goodness of fit is given by

$$r = \frac{\sum_{i=1}^{n} (M_{\infty_i} - \bar{M}_\infty)(C_{p_i} - \bar{C}_p)}{\sqrt{\sum_{i=1}^{n} (M_{\infty_i} - \bar{M}_\infty)^2 \sum_{i=1}^{n} (C_{p_i} - \bar{C}_p)^2}} \qquad \text{(A4)}$$

where if $r = 0$ there is no correlation and if $|r| = 1$ then there is perfect correlation. For the present analysis if $|r| > 0.5$, then the correlation is considered strong enough to use m in correcting a given M_∞ to another value. If $|r| < 0.5$, the dependence between C_p and M_∞ is considered weak, and m is assumed to be zero. Three examples of various values of r are shown in figure 41 for the $M_\infty = 0.85$ and $R_c = 16$ million path. Figure 41(a) shows the value of C_p for $x/c = 0.00$ (the orifice at the leading edge of the airfoil) as a function of M_∞. In this case $r = 0.15$ and, indeed, there seems to be little correlation between M_∞ and C_p. Consequently, no attempt is made to manipulate or correct this data for small differences in M_∞. Figure 41(b) shows the values of C_p for $x/c = 0.40$ as a function of M_∞. In this case $r = 0.49$, and so this linear curve fit barely fails to meet the correlation test. Figure 41(c) illustrates the values of C_p for $x/c = 0.80$ that lead to a value of r equal to 0.92. As seen in figure 41(c), there is good correlation between C_p and M_∞, and differences in C_p due to differences in M_∞ can be removed by correcting values of C_p to a given M_{∞_o} by setting

$$C_{p_o} = C_p - m \cdot (M_\infty - M_{\infty_o}) \tag{A5}$$

where C_{p_o} is the corrected value of C_p and m is the slope of the linear fit. Again, m is assumed to be equal to zero if $|r| < 0.5$.

Once the linear regression technique has been applied to the values of C_p for each orifice along the path, a set of intermediate graphs are drawn before the airfoil onset T_t is determined. For each orifice a value of ΔC_p is plotted as a function of T_t where

$$\Delta C_p = C_{p_o} - C_{p_{ave}} \tag{A6}$$

In equation (A6), C_{p_o} is corrected with respect to M_∞ and $C_{p_{ave}}$ is an average of condensation-free values of C_{p_o} for that orifice. (Condensation-free values were determined by establishing crude onset values of T_t without the benefit of correction procedures and then adding at least a 2 K temperature buffer. Final onset values of T_t were then checked to insure that $C_{p_{ave}}$ was indeed free from condensation effects.) An example of a ΔC_p vs. T_t

with and without correction is shown in figure 42 for $x/c = 0.80$ and where $r = 0.92$. Figure 42(a) shows the uncorrected data while figure 42(b) shows the values of C_p after being corrected. As can be seen, considerable "order" is added to the data by the correction process and this "order" permits easier identification of the T_t at which C_p at this x/c location begins to depart from its unaffected average value. Not always, however, was $|r| > .5$ and so this simplification was not always possible. Graphs similar to figures 42(a) or 42(b) are then drawn for each orifice location over the airfoil. These graphs are used to determine at what T_t each of the orifices first experience systematic departure from its unaffected average value of C_{p_o}.

These orifice onset temperatures are then plotted as a function of x/c as was shown in figure 20. These orifice onset T_t vs. x/c plots are the key analysis graphs because they provide an overview of the effects on the airfoil as a whole. There is experimental uncertainty in the onset point for each orifice and consequently it is helpful to see all of the orifice onset T_t's together so that a particularly low or high value can be checked for possible error. The airfoil onset T_t is not taken to be an average of orifice onset T_t's, but rather is taken to be the warmest orifice onset T_t that appears systematic. Uncertainty bars are normally drawn to encompass the highest orifice onset T_t, whether the deviation appears systematic or not.

The data analysis procedure described herein was more sensitive to condensation onset than previous analyses described in references 17, 18 and 19. In references 17 and 18 pressure distributions were superimposed to detect differences - no correction was made to C_p for differences in M_∞ and, consequently, much of the data could not be used. Reference 19 utilized the ΔC_p vs. T_t format at 0, 25, 50, and 75 percent chord locations but still did not include the Mach correction technique.

APPENDIX B

ERROR ANALYSIS FOR ΔC_p VS. T_t GRAPHS

During the present experiment, fluctuations in wind tunnel conditions were the prime source of error during the 50 second period required to record the data. Tunnel conditions were observed to fluctuate with standard deviations of the following approximate magnitudes: σ_{p_t} of +.005 atm (varied with M_∞ and R_c); σ_{M_∞} of ±.003; and σ_{T_t} of ±0.5 K. The manufacturer's stated uncertainty in the static pressure measurements, Δp, was 0.5% of full scale. A representative standard deviation for ΔC_p due to these fluctuations is calculated herein using normal error propagation techniques, see reference 20 for example.

As defined in equation (A6),

$$\Delta C_p = C_{p_o} - C_{p_{ave}} \qquad \text{(A6)}$$

in which C_{p_o} is the value of the pressure coefficient, corrected to some value of free-stream Mach number, M_{∞_o}, from data taken at a free-stream Mach number of M_∞. The correction is defined as

$$C_{p_o} = C_p - m \cdot (M_\infty - M_{\infty_o}) \qquad \text{(A5)}$$

where m is the slope of the linear regression fit as defined in equation (A1). If sufficient correlation, r, as defined in equation (A4), is not found, m is assumed to be equal zero. Since $C_{p_{ave}}$ is just the average of the corrected condensation-free data, the variance of $C_{p_{ave}}$ can be approximated by

$$\sigma^2_{C_{p_{ave}}} = \frac{\sigma^2_{C_{p_o}}}{N} \qquad (B1)$$

where N would be the number of samples used in the average. The variance of C_{p_o} can be written from equation (A5) as

$$\sigma^2_{C_{p_o}} = \sigma^2_{C_p} + \sigma^2_F \qquad (B2)$$

where F is defined as

$$F = m(M_\infty - M_{\infty_o}) \qquad (B3)$$

Assuming there is much more relative error in $(M_\infty - M_{\infty_o})$ than m, the variance in F will be primarily due to the variance in the difference in Mach numbers. Since M_{∞_o} is an arbitrarily defined constant, we may write

$$\sigma^2_F = m^2\sigma^2_{M_\infty} \qquad (B4)$$

Consequently, equations (A5), (A6), (B1), (B2), and (B3) lead to

$$\sigma^2_{\Delta C_p} = \left(\frac{N + 1}{N}\right)(\sigma^2_{C_p} + m^2\sigma^2_{M_\infty}) \qquad (B5)$$

It now remains to discuss $\sigma^2_{C_p}$, the variance associated with error in the values of C_p before Mach correction. The value of C_p is defined as

$$C_p = \frac{p - p_\infty}{q_\infty} \qquad (B6)$$

Though C_p is strictly a function of R and M as Schlichting explains in reference 21, the calculated value of C_p from an experiment may be sensitive to errors or fluctuations in p, p_t, T_t, and M_∞. In other words, one must distinguish between actual C_p, C_p (act), and calculated C_p, C_p (cal). During the present experiment, the prime difference between C_p (act) and C_p (cal) was lack of simultaneity - tunnel conditions were recorded at some time t and the static value of p at an orifice may have been recorded at a time up to 50 seconds later. Calculation of the impact of all the fluctuations upon the possible error in C_p (cal) will be presented below except for the dependence of C_p (cal) on T_t. Since T_t only enters the dependence of C_p (cal) through R, and since the R dependence was weak, no error in C_p due to T_t was calculated. An equation for the variance of C_p can be written as

$$\sigma^2_{C_p}\ (\text{cal}) = \left(\frac{\partial C_p}{\partial p_t}\right)^2 \sigma^2_{p_t} + \left(\frac{\partial C_p}{\partial M_\infty}\right)^2 \sigma^2_{M_\infty} + \left(\frac{\partial C_p}{\partial \Delta p}\right)^2 \sigma^2_{\Delta p} \qquad \text{(B7)}$$

The next three sub-sections describe the calculation of the partial derivatives.

$$\text{Solving for } \left.\frac{\partial C_p(\text{cal})}{\partial p_t}\right|_{M_\infty,\ R,\ \frac{x}{c}}$$

Equation (B6) can be rewritten as

$$C_p(\text{act}) = \frac{\frac{p}{p_t} - \frac{p_\infty}{p_t}}{\frac{q_\infty}{p_t}} \qquad \text{(B8)}$$

Since M_∞ and R are held constant during the process, then C_p(act), $\frac{p_\infty}{p_t}$, and $\frac{q_\infty}{p_t}$ all remain constant. Thus for a p_t fluctuation, equation (B8) yields.

$$\frac{p}{p_t} = \text{Constant} \tag{B9}$$

or that

$$\frac{\partial p}{\partial p_t}\Big|_{M_\infty,\ R,\ \frac{x}{c}} = \frac{p}{p_t} \tag{B10}$$

Now, turning back to C_p(cal) and remembering that p_t, p_∞ and thus q_∞ are all recorded at some time t_1 and then p is recorded later at some t, equation (B8) can be written as

$$C_p(\text{cal}) = \frac{\frac{p}{p_{t_1}} - \frac{p_{\infty_1}}{p_{t_1}}}{\frac{q_{\infty_1}}{p_{t_1}}} \tag{B11}$$

so that

$$\frac{\partial C_p(\text{cal})}{\partial p_t}\Big|_{M_\infty,\ R,\ \frac{x}{c}} = \frac{1}{q_{\infty_1}} \frac{\partial p}{\partial p_t}\Big|_{M_\infty,\ R,\ \frac{x}{c}} \tag{B12}$$

or with equation (B10) and dropping the subscripts "1"

$$\frac{\partial C_p(\text{cal})}{\partial p_t}\Big|_{M_\infty,\ R,\ \frac{x}{c}} = \frac{p}{q_\infty p_t} \tag{B13}$$

Assuming the isentropic relation for a perfect gas with its ratio of specific heats equal to 1.4, equation (B13) can be written as

$$\left.\frac{\partial C_p(\text{cal})}{\partial p_t}\right|_{M_\infty, R, \frac{x}{c}} = \frac{1}{p_t}\left(C_p + \frac{1}{.7M_\infty^2}\right) \tag{B14}$$

Solving for $\left.\frac{\partial C_p(\text{cal})}{\partial M_\infty}\right|_{p_t, R, \frac{x}{c}}$

This partial derivative is found when the linear regression step in the Mach correction technique is performed as outlined in appendix A. The value of $\frac{\partial C_p(\text{cal})}{\partial M_\infty}$ is equal to the value of the slope, m,

$$\frac{\partial C_p(\text{cal})}{\partial M_\infty} = m \tag{B15}$$

because m is just the linear regression fit to calculated values of C_p as a function of M_∞. As before, when the correlation coefficient, r, does not reflect good correlation, then $\frac{\partial C_p(\text{cal})}{\partial M_\infty}$, like m, will be assumed equal to zero.

Solving for $\left.\frac{\partial C_p}{\partial \Delta p}\right|_{p_t, M_\infty, R, \frac{x}{c}}$

This is just the simple case where $C_p(\text{cal})$ is in error because of instrument error in p. That is,

$$p(\text{cal}) = p(\text{act}) + \Delta p \tag{B16}$$

so

$$\left.\frac{\partial p}{\partial \Delta p}\right|_{p_t, M_\infty, R, \frac{x}{c}} = 1$$

Consequently,

$$\frac{\partial C_p(\text{cal})}{\partial \Delta p} = \frac{1}{q_\infty} \tag{B17}$$

or in terms of M_∞ and p_t for the isentropic flow of a perfect gas with a ratio of specific heats equal to 1.4

$$\frac{\partial C_p(\text{cal})}{\partial \Delta p} = \frac{\left(1 + \frac{M_\infty^2}{5}\right)^{3.5}}{.7 p_t M_\infty^2} \tag{B18}$$

At this point, all of the partial derivatives in equation (B7) are known and can be combined with the observed or known values of σ_{p_t}, σ_{M_∞}, and $\sigma_{\Delta p}$. The value of $\sigma_{\Delta p}$ was first taken to be the manufacturer's value of 0.5 percent of full scale, but this value gave a contribution to the error bar in C_p that was on the order of 10 times the actual fluctuations in C_p. Apparently the two pressure transducers performed with much better precision than expected. In fact, instead of the expected respective uncertainties of 0.0170 and 0.0085 atm for the M_∞ = 0.75, 0.95 and the M_∞ = 0.85 tests, the uncertainties were on the order of .0004 and .0002 atm, respectively. These low magnitudes in $\sigma_{\Delta p}$ made the contribution of the instrument error to the total error negligible.

Assuming isentropic relations for a perfect gas with the ratio of specific heats equal to 1.4 and assuming $\sigma_{\Delta p}$ is negligible, equations (B5), (B7), (B14), and (B15) can be combined to give

$$\sigma_{\Delta C_p}^2 = \left(\frac{N+1}{N}\right) \left\{ \left[\left(C_p + \frac{1}{.7 M_\infty^2}\right)/P_t\right]^2 \sigma^2_{p_t} + 2\, m^2\, \sigma^2_{M_\infty} \right\} \tag{B20}$$

The error bars used in the ΔC_p vs. T_t graphs in the data analysis procedure were calculated with the above value of $\sigma_{\Delta C_p}$.

REFERENCES

1. Adcock, Jerry B.: Real-Gas Effects Associated with One-Dimensional Transonic Flow of Cryogenic Nitrogen. NASA TN D-8274, 1976.

2. Wegener, P. P.; and Mack, L. M.: Condensation in Supersonic and Hypersonic Wind Tunnels. Advances in Applied Mechanics, Vol. V, 1958, pp. 307-447.

3. Wegener, Peter P.: Nonequilibrium Flow with Condensation. Acta-Mechanica 21, 1975, pp. 65-91.

4. Daum, Fred L.; and Gyarmathy, George: Condensation of Air and Nitrogen in Hypersonic Wind Tunnels. AIAA Journal, Vol. 6, No. 3, Mar. 1968, pp. 458-465.

5. Goglia, Gennaro L.; and Van Wylen, Gordon J.: Experimental Determination of Limit of Supersaturation of Nitrogen Vapor Expanding in a Nozzle. Journal of Heat Transfer, Vol. 83, Series C, No. 1, Feb. 1961, pp. 27-32.

6. Arthur, P. D.; and Nagamatsu, H. T.: Effects of Impurities on the Supersaturation of Nitrogen in a Hypersonic Nozzle. Hypersonic Wind Tunnel Mem. No. 7, Guggenheim Aeronaut. Lab., Calif. Inst. of Technol., Pasadena, California, 1952.

7. Adcock, Jerry B.; and Ogburn, Marilyn E.: Power Calculations for Isentropic Compressions of Cryogenic Nitrogen. NASA TN D-8389, 1977.

8. Kilgore, Robert A: The Cryogenic Wind Tunnel for High Reynolds Number Testing. Ph. D. Thesis, University of Southampton, 1974.

9. Kilgore, Robert A.: Design Features and Operational Characteristics of the Langley Pilot Transonic Cryogenic Tunnel. NASA TM X-72012, 1974.

10. Stauffer, D.: Kinetic Theory of Two-Component ("Heteromolecular") Nucleation and Condensation. J. Aerosol Sci., Vol. 7, 1976, pp. 319-333.

11. Wegener, Peter P.; and Wu, Benjamin, J. C.: Homogeneous and Binary Nucleation: New Experimental Results and Comparisons with Theory. Faraday Discussions of the Chemical Society, No. 61 Precipitation, 1976.

12. Wilemski, Gerald: Binary Nucleation. I. Theory Applied to Water-Ethanol Vapors. Journal of Chemical Physics. Vol. 62, No. 9, May 1975, pp. 3763-3771.

13. Wilemski, Gerald: Binary Nucleation. II. Time Lags. Journal of Chemical Physics, Vol. 62, No. 9, May 1975, pp. 3772-3776.

14. Sivier, Kenneth D.: Digital Computer Studies of Condensation in Expanding One-Component Flows. Aerospace Research Laboratories Report ARL 65-234, November 1965.

15. Goglia, Gennaro L.: Limit of Supersaturation of Nitrogen Vapor Expanding in a Nozzle. Ph. D. Thesis, University of Michigan, 1959.

16. Freund, John E.: Mathematical Statistics. Second ed. Prentice-Hall, Inc., 1971.

17. Hall, Robert M.: Preliminary Study of the Minimum Temperatures for Valid Testing in a Cryogenic Wind Tunnel. NASA TM X-72700, 1975.

18. Hall, Robert M.; and Ray, Edward J.: Investigation of Minimum Operating Temperatures for Cryogenic Wind Tunnels. Journal of Aircraft, Vol. 14, No. 6, June 1977, pp. 560-564.

19. Hall, Robert M.: An Analysis of Data Related to the Minimum Temperatures for Valid Testing in Cryogenic Wind Tunnels Using Nitrogen as the Test Gas. NASA TM X-73924, 1976.

20. Crandall, Keith C.; and Seabloom, Robert W.: Engineering Fundamentals in Measurements, Probability, Statistics, and Dimensions. McGraw-Hill, 1970.

21. Schlichting, Hermann: Boundary-Layer Theory. Sixth ed. McGraw-Hill, 1968.

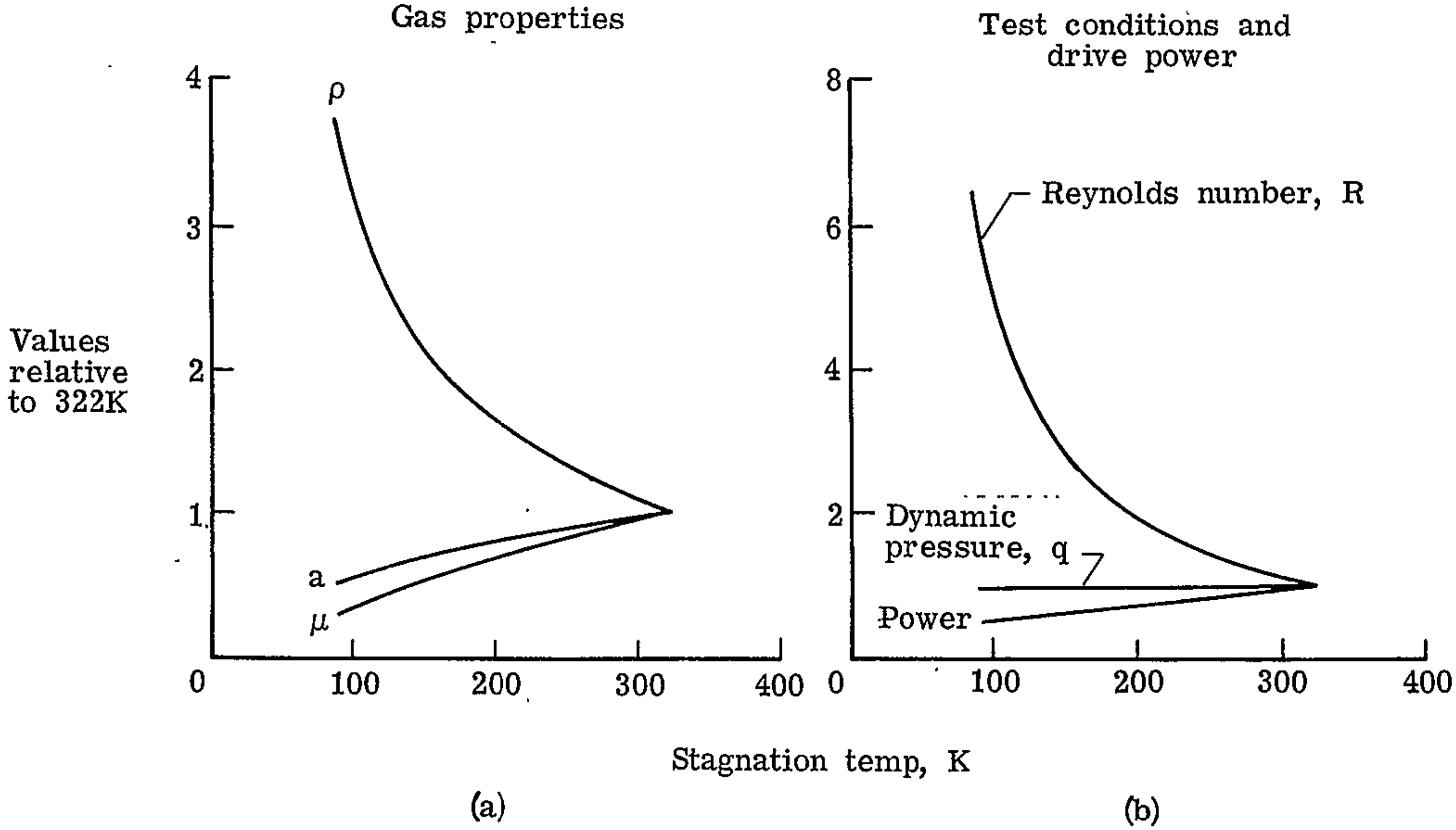

Figure 1.- Effect of temperature reduction for $M_\infty = 1.0$, constant P_t, and constant reference length.

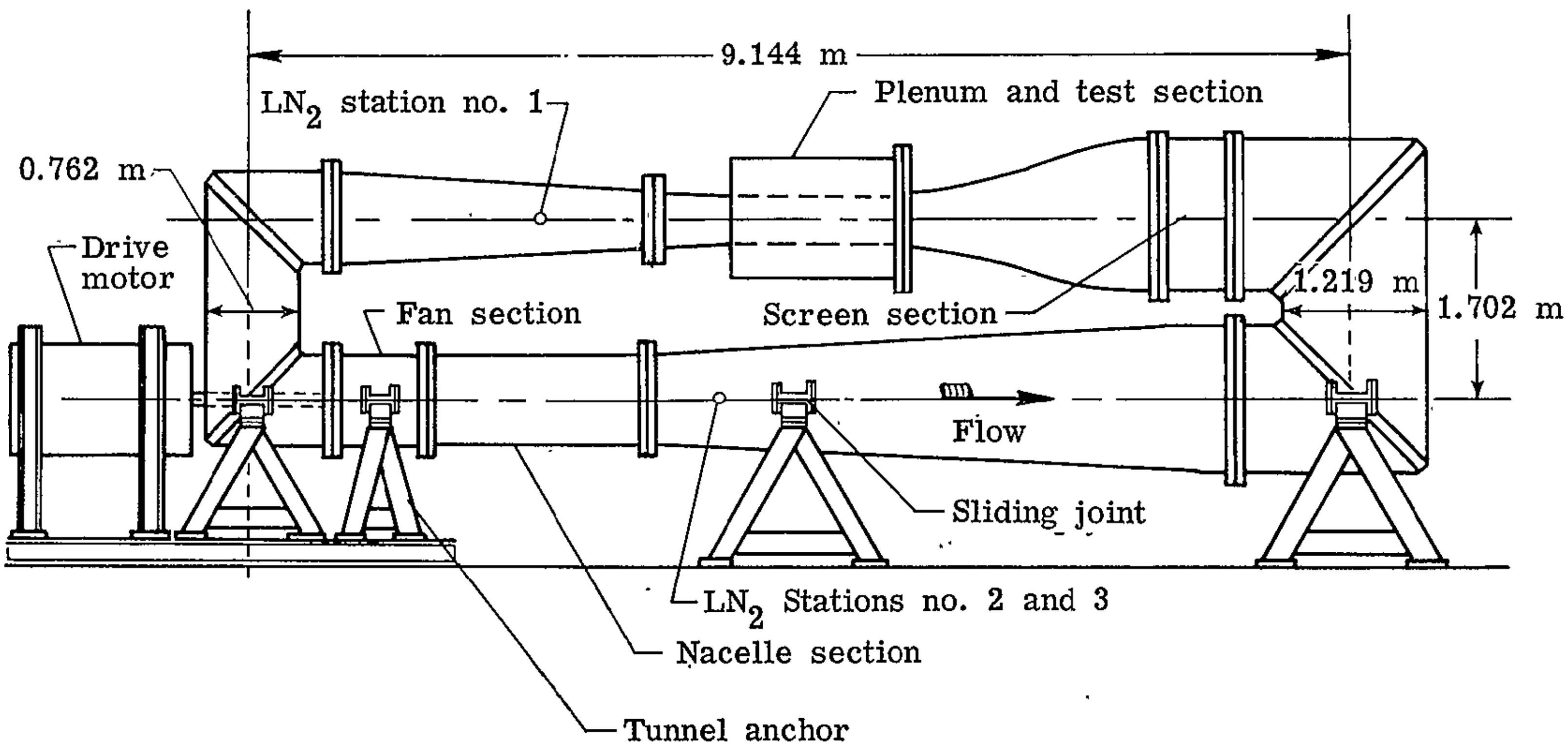

Figure 2.- Schematic of Langley 0.3-m transonic cryogenic tunnel.

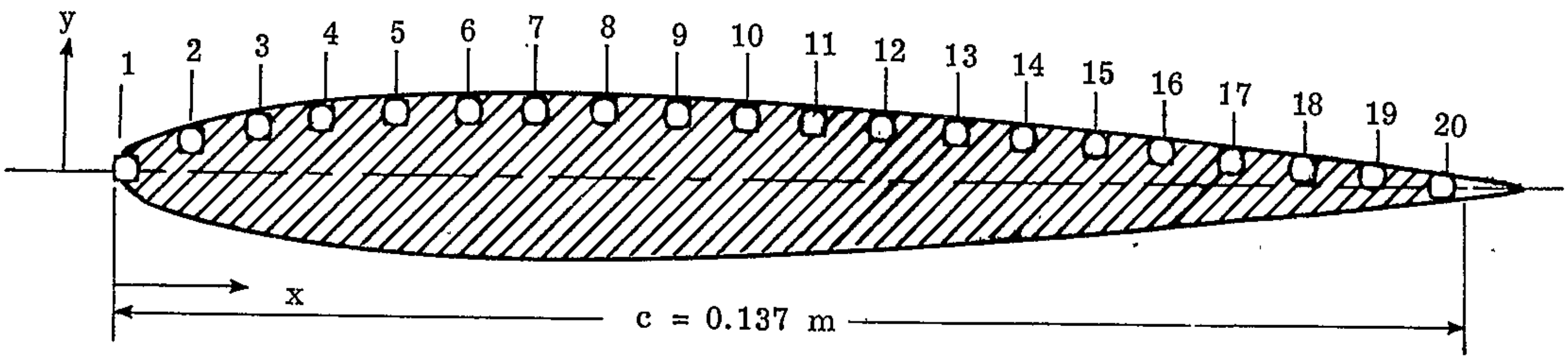

Figure 3.- Two dimensional NACA 0012-64 airfoil has orifices spaced at 5 % chord locations. Trailing edge orifice was added for tests with M_∞ = 0.75 and 0.95.

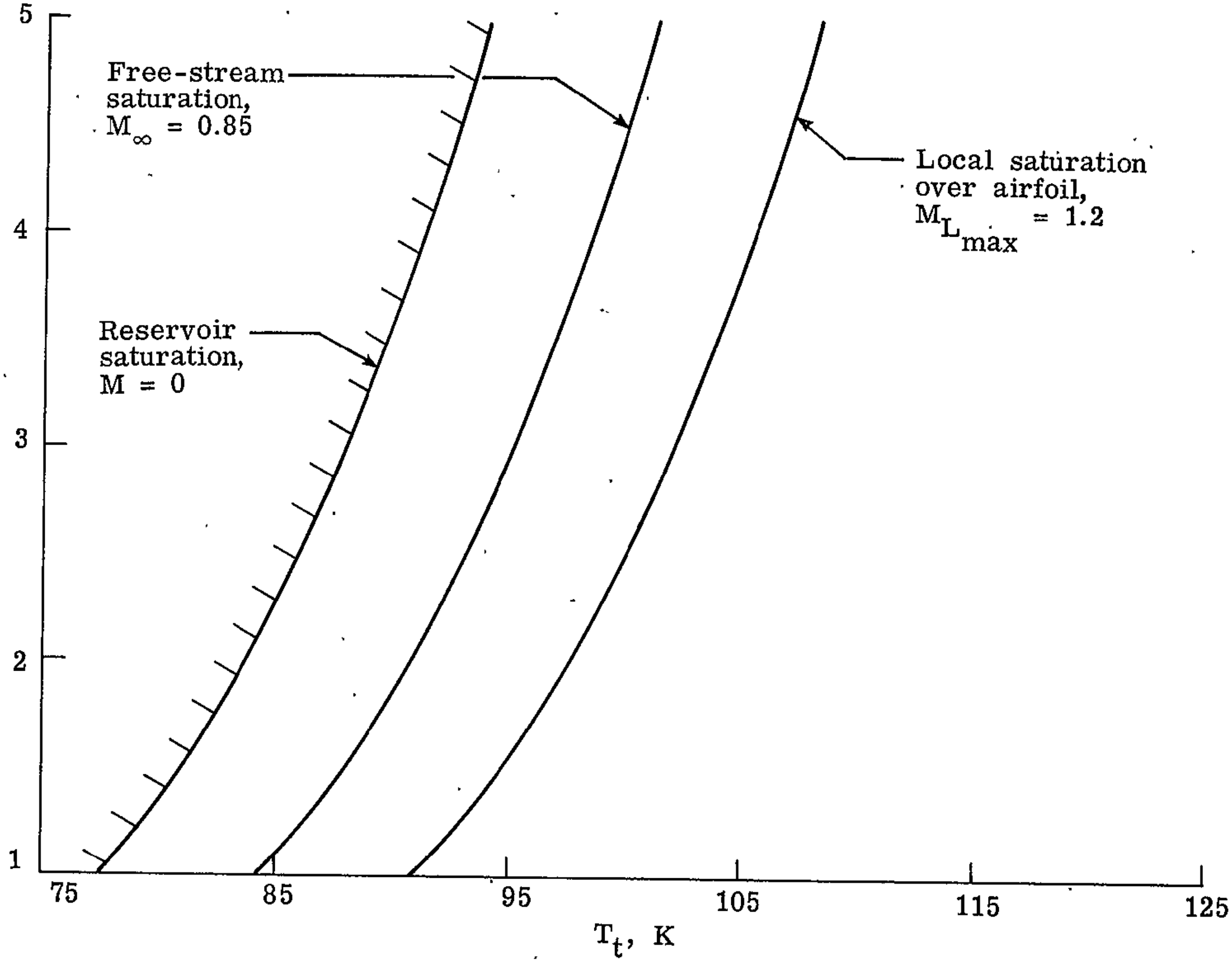

Figure 4.- Region of interest for the M_∞ = 0.85 test.

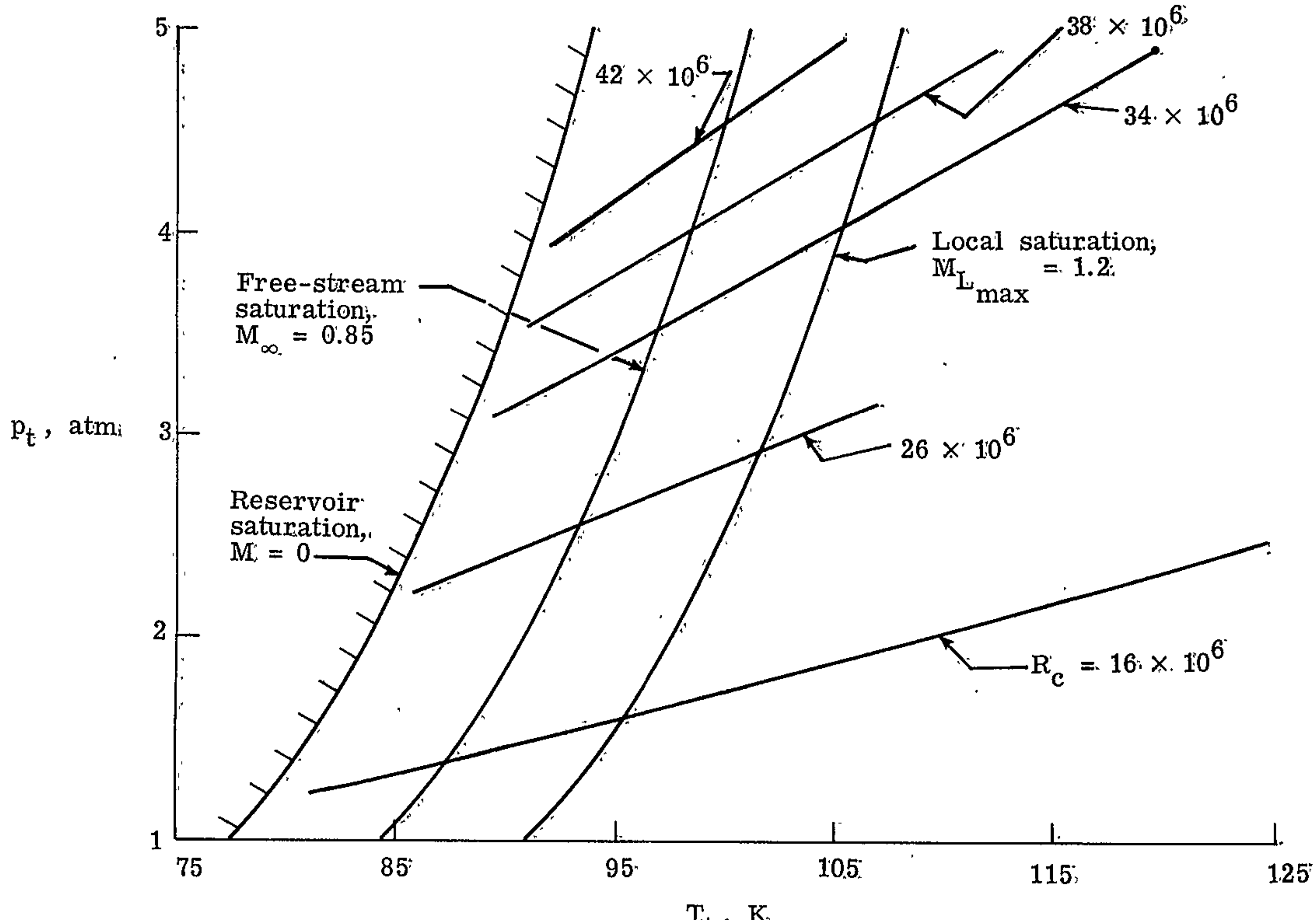

Figure 5.- Path of constant $\bar{R}_c$ for the $M_\infty = 0.85$ test.

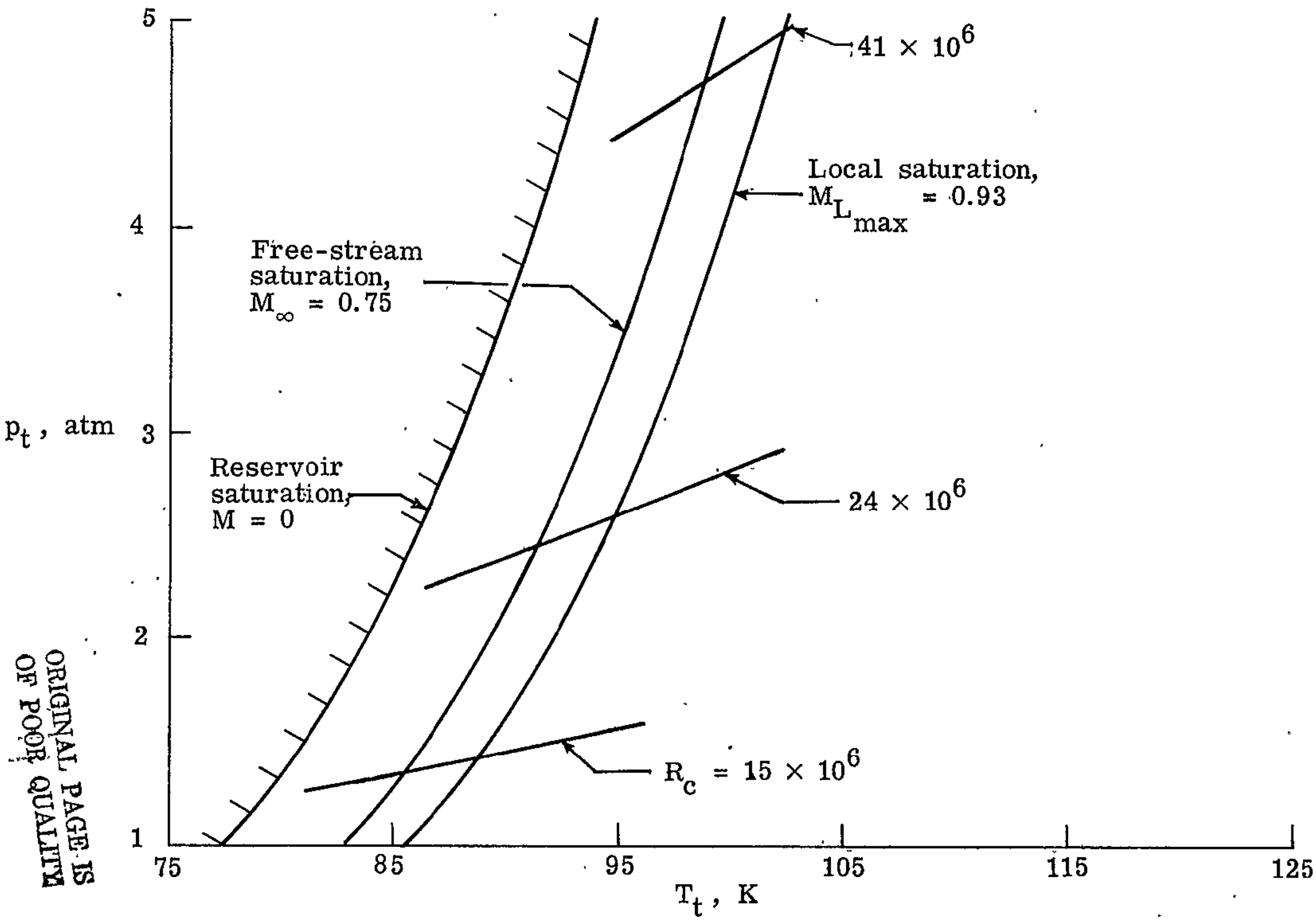

Figure 6.- Paths of constant R_c for the M_∞ = 0.75 test.

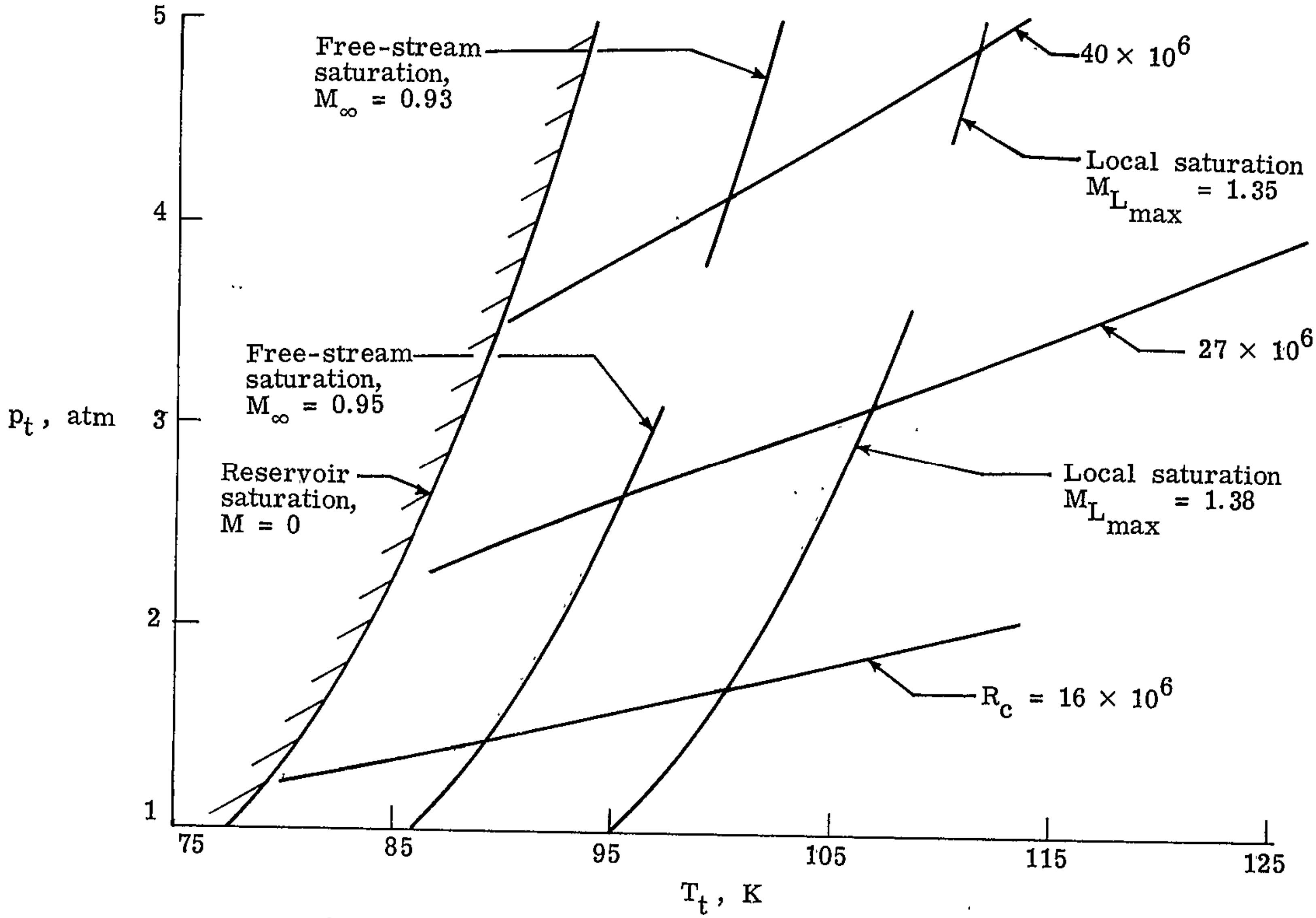

Figure 7.- Paths of constant R_c for the $M_\infty = 0.95$ test. ($R_c = 40 \times 10^6$ path taken with $M_\infty = 0.93$.)

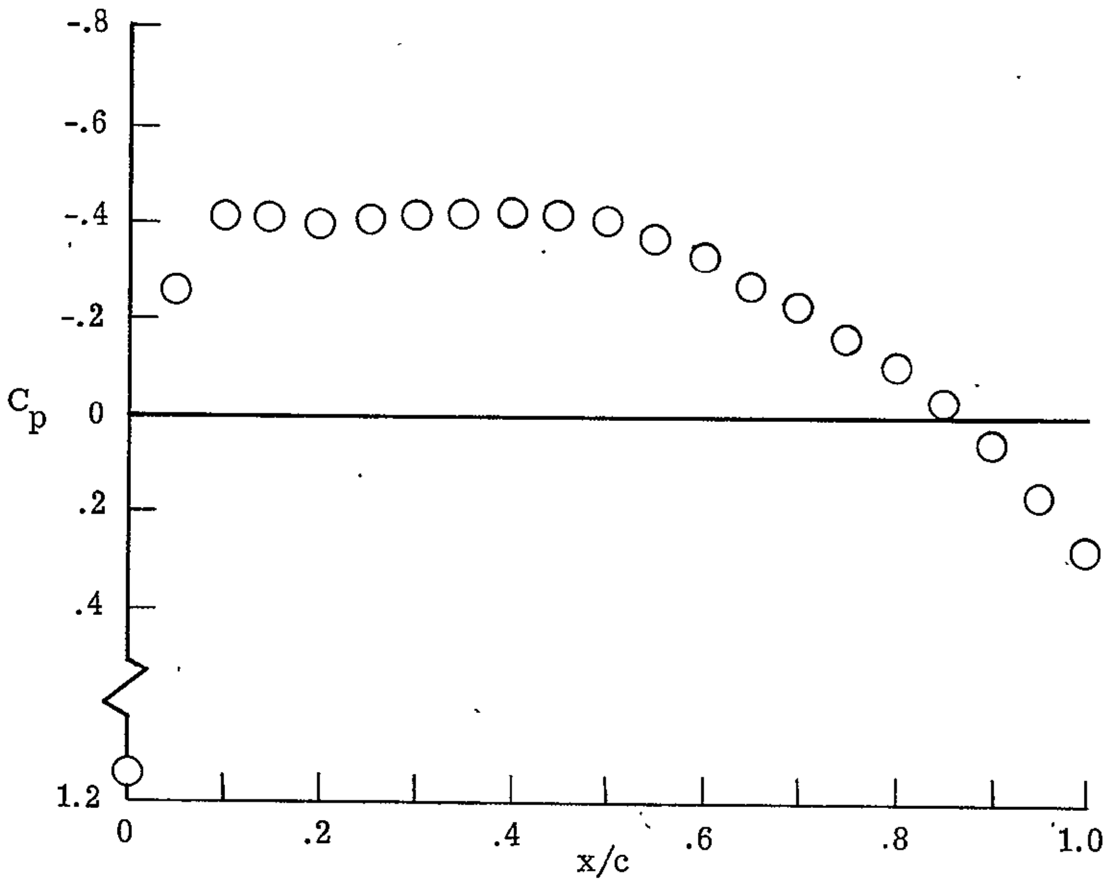

Figure 8.- Average unaffected pressure distribution for the $R_c = 15 \times 10^6$ path of the $M_\infty = 0.75$ test.

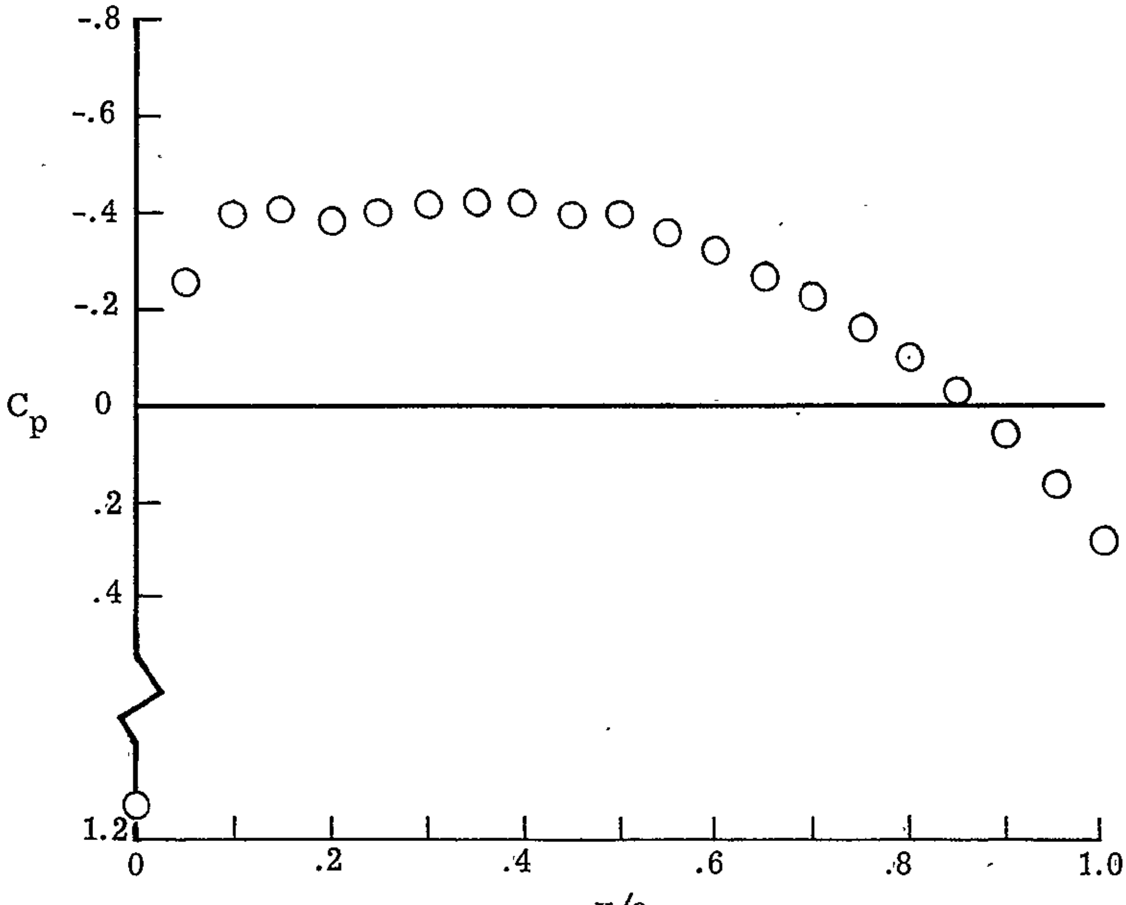

Figure 9.- Average unaffected pressure distribution for the $R_c = 24 \times 10^6$ path of the $M_\infty = 0.75$ test.

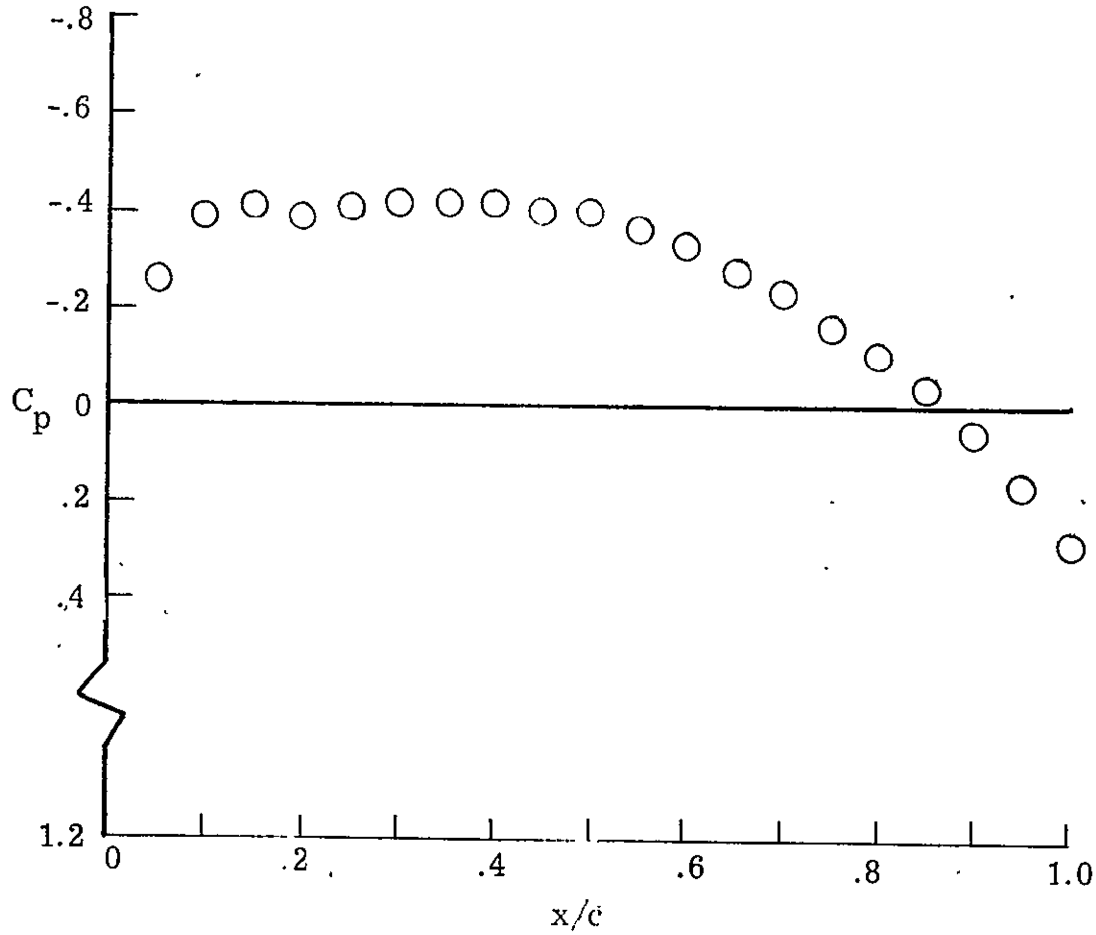

Figure 10.- Average unaffected pressure distribution for the $R_c = 41 \times 10^6$ path of the $M_\infty = 0.75$ test.

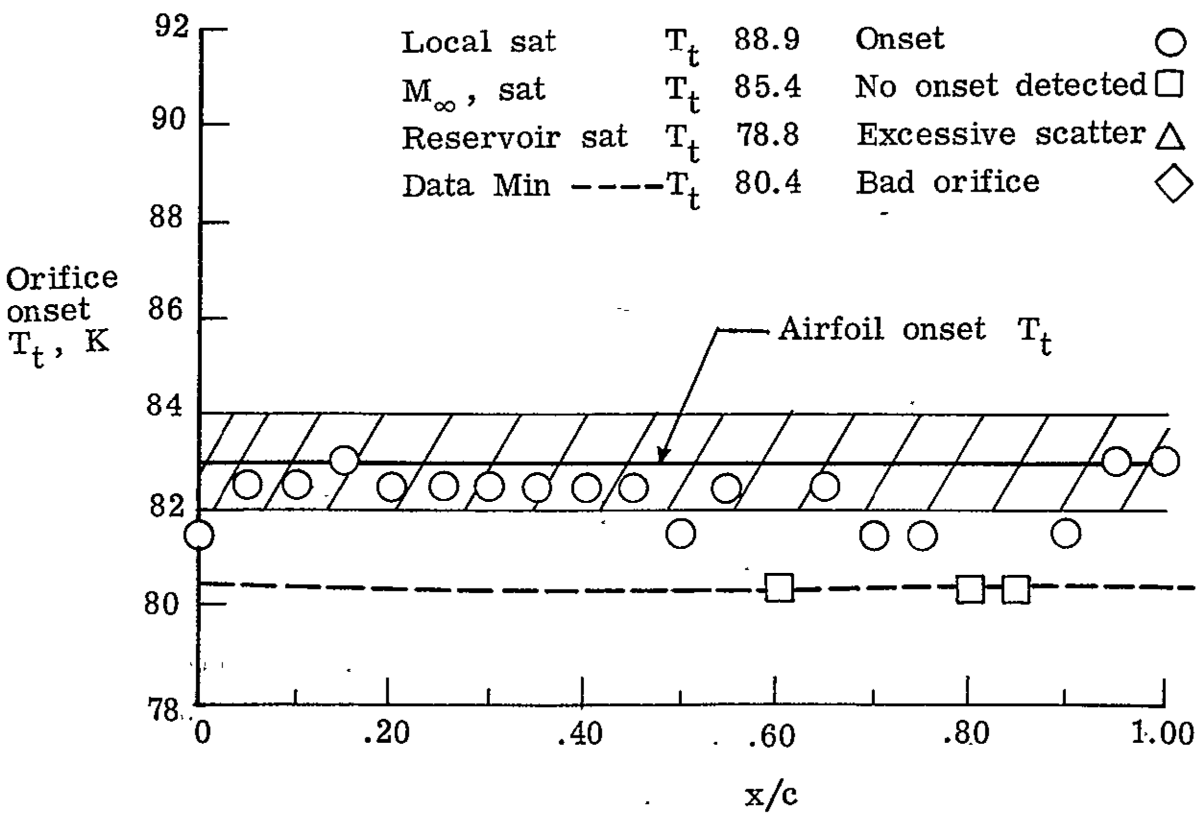

Figure 11.- Orifice onset T_t's and resulting airfoil onset $\bar{T}_t$ for the $R_c = 15 \times 10^6$ path of the $M_\infty = 0.75$ test.

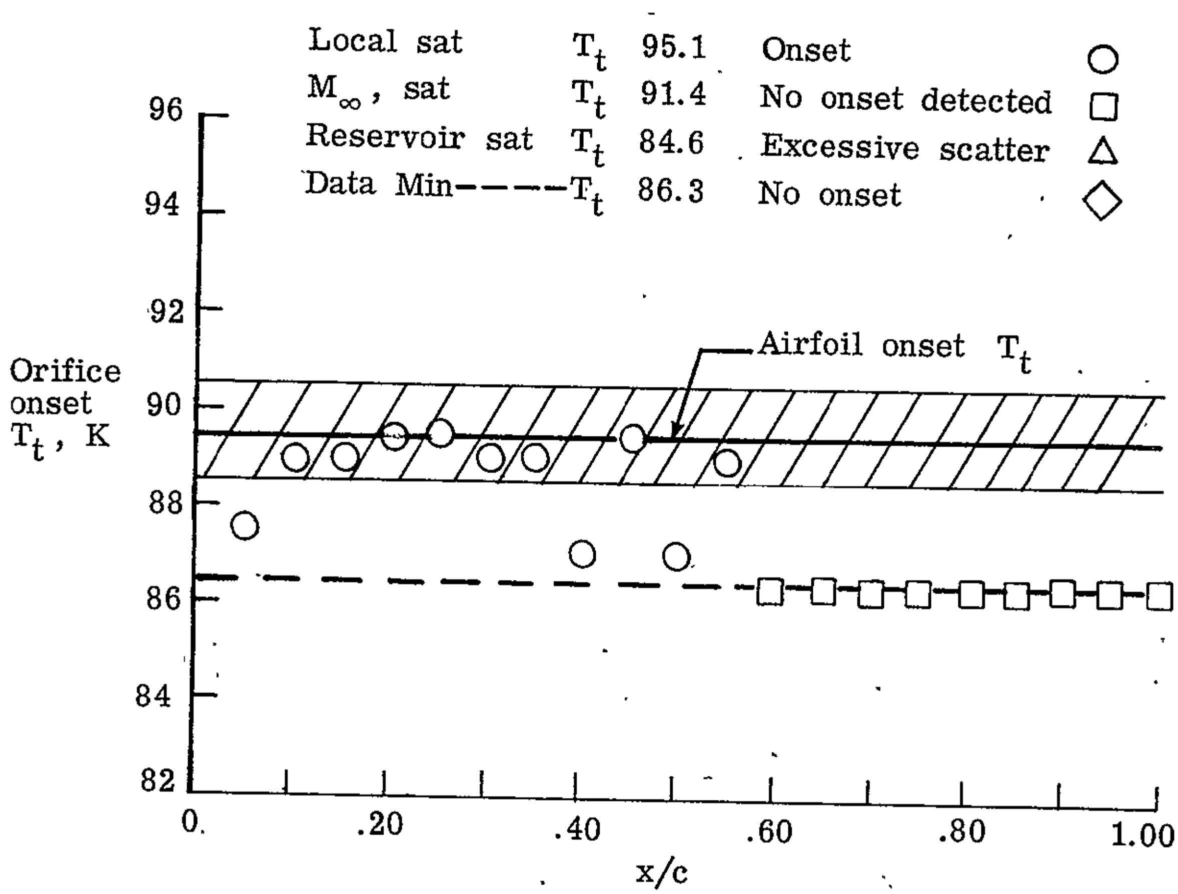

Figure 12.- Orifice onset T_t's and resulting airfoil onset T_t for the $R_c = 24 \times 10^6$ path of the $M_\infty = 0.75$ test.

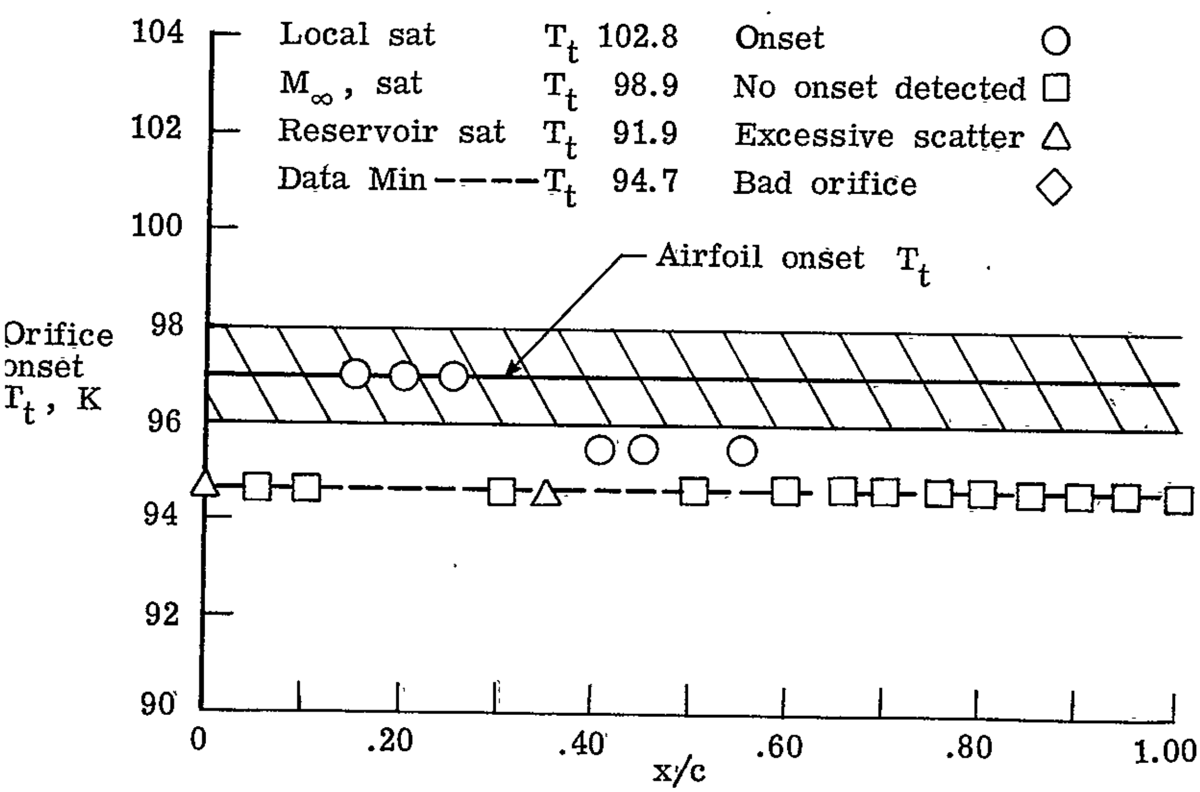

Figure 13.- Orifice onset T_t's and resulting airfoil onset T_t for the $R_c = 41 \times 10^6$ path of the $M_\infty = 0.75$ test.

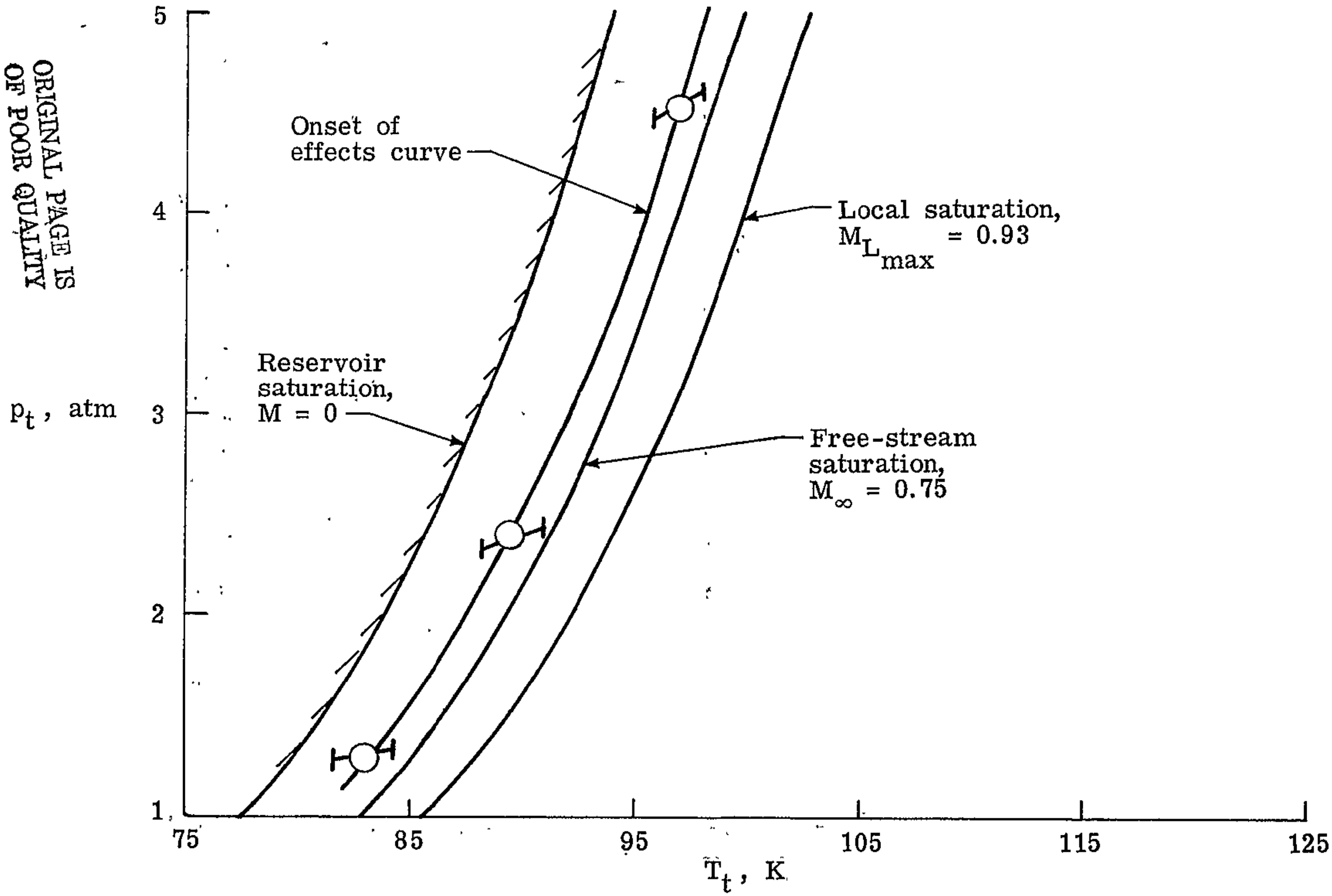

Figure 14.- Onset of condensation effects for M_∞ = 0.75 test.

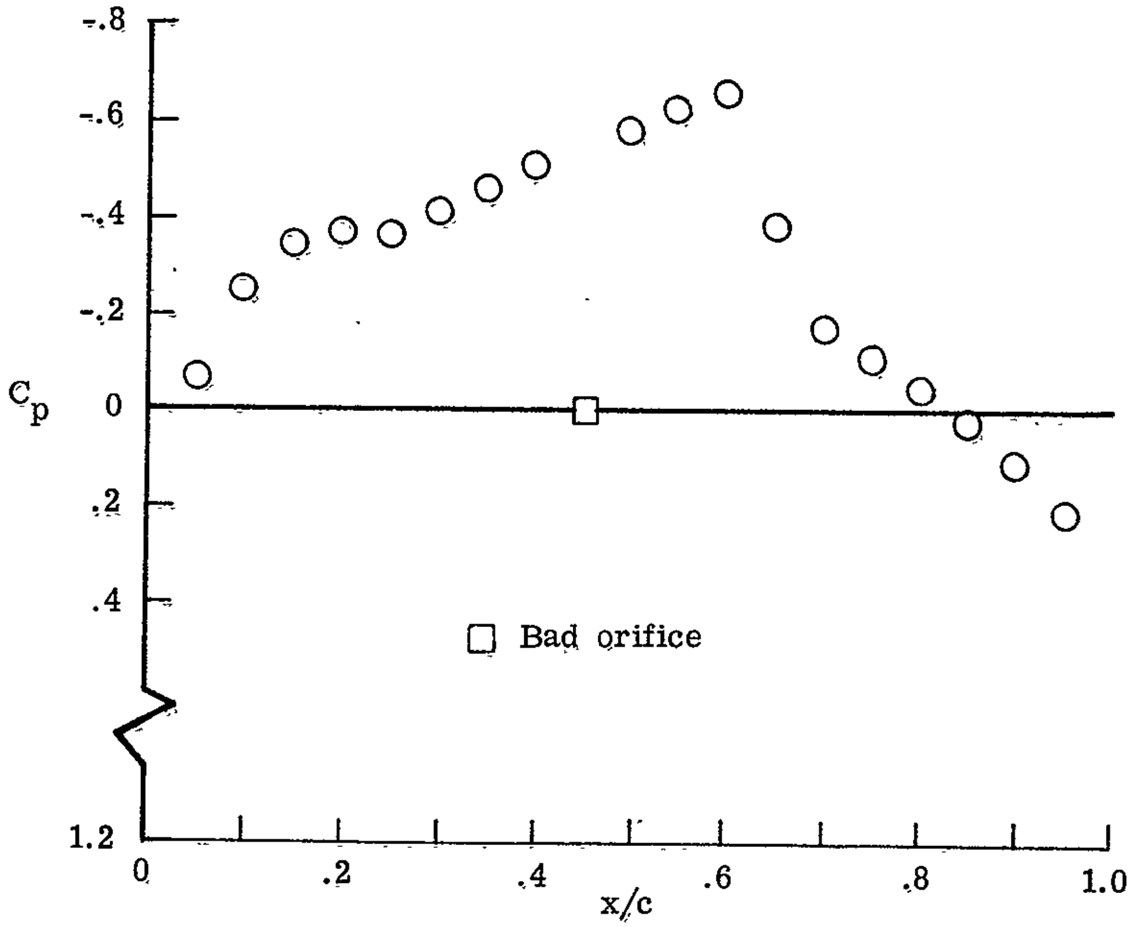

Figure 15.- Average unaffected pressure distributon for the $R_c = 16 \times 10^6$ path of the $M_\infty = 0.85$ test.

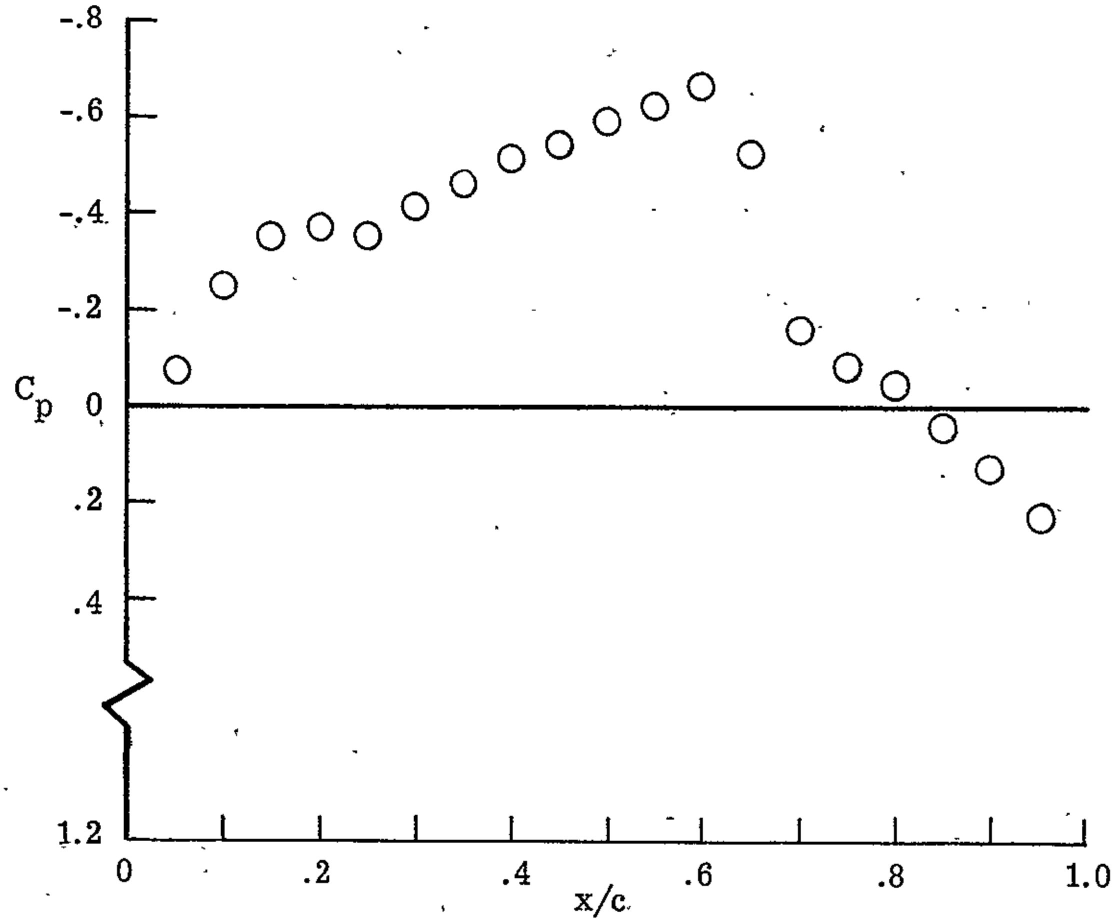

Figure 16.- Average unaffected pressure distribution for the $R_c = 26 \times 10^6$ path of the $M_\infty = 0.85$ test.

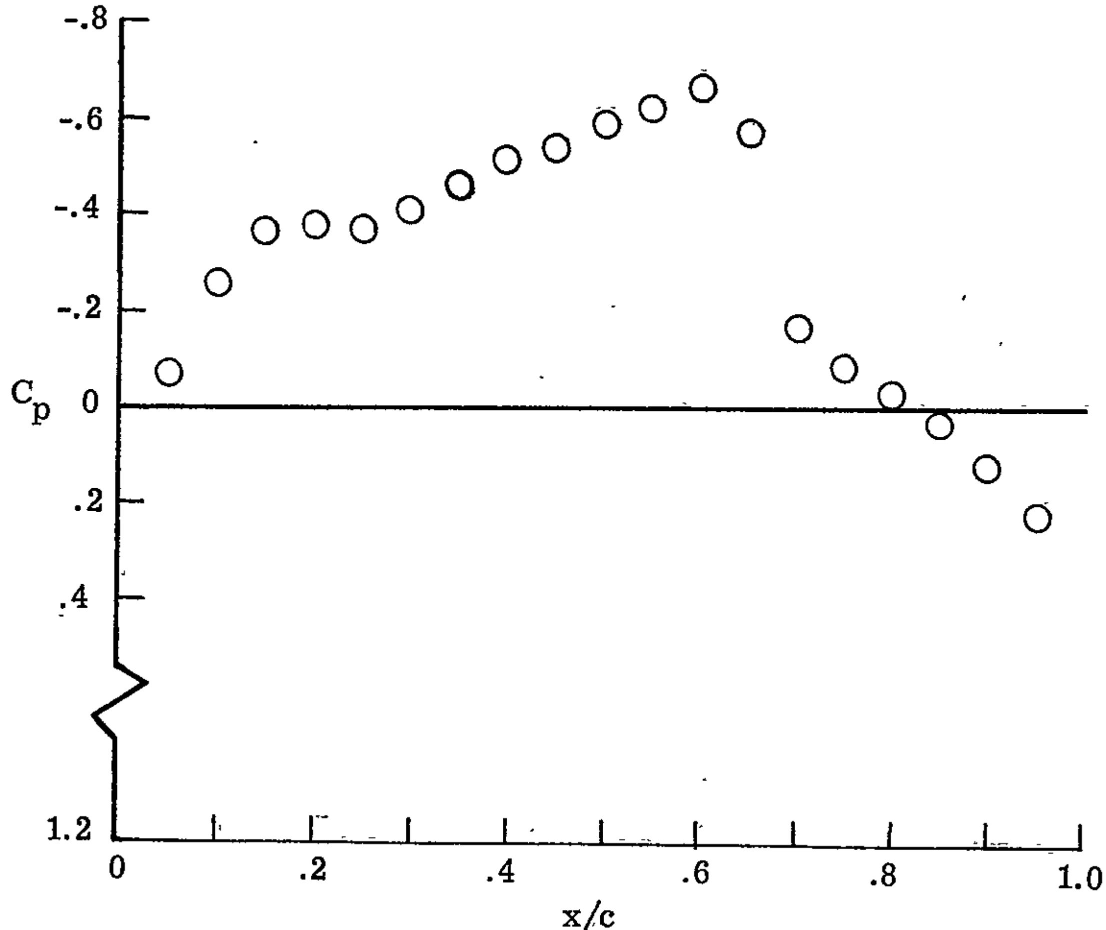

Figure 17.- Average unaffected pressure distribution for the $R_c = 34 \times 10^6$ path of the $M_\infty = 0.85$ test.

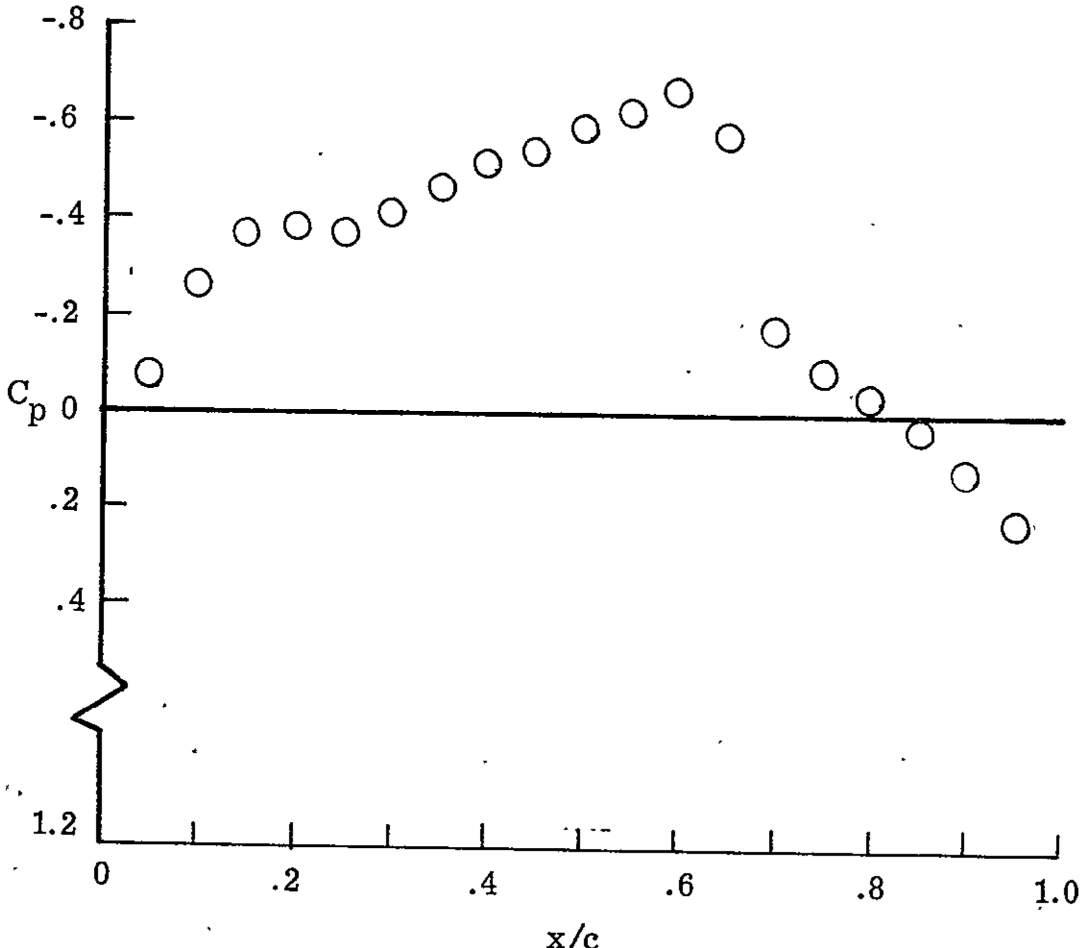

Figure 18.- Average unaffected pressure distribution for the $R_c = 38 \times 10^6$ path of the $M_\infty = 0.85$ test.

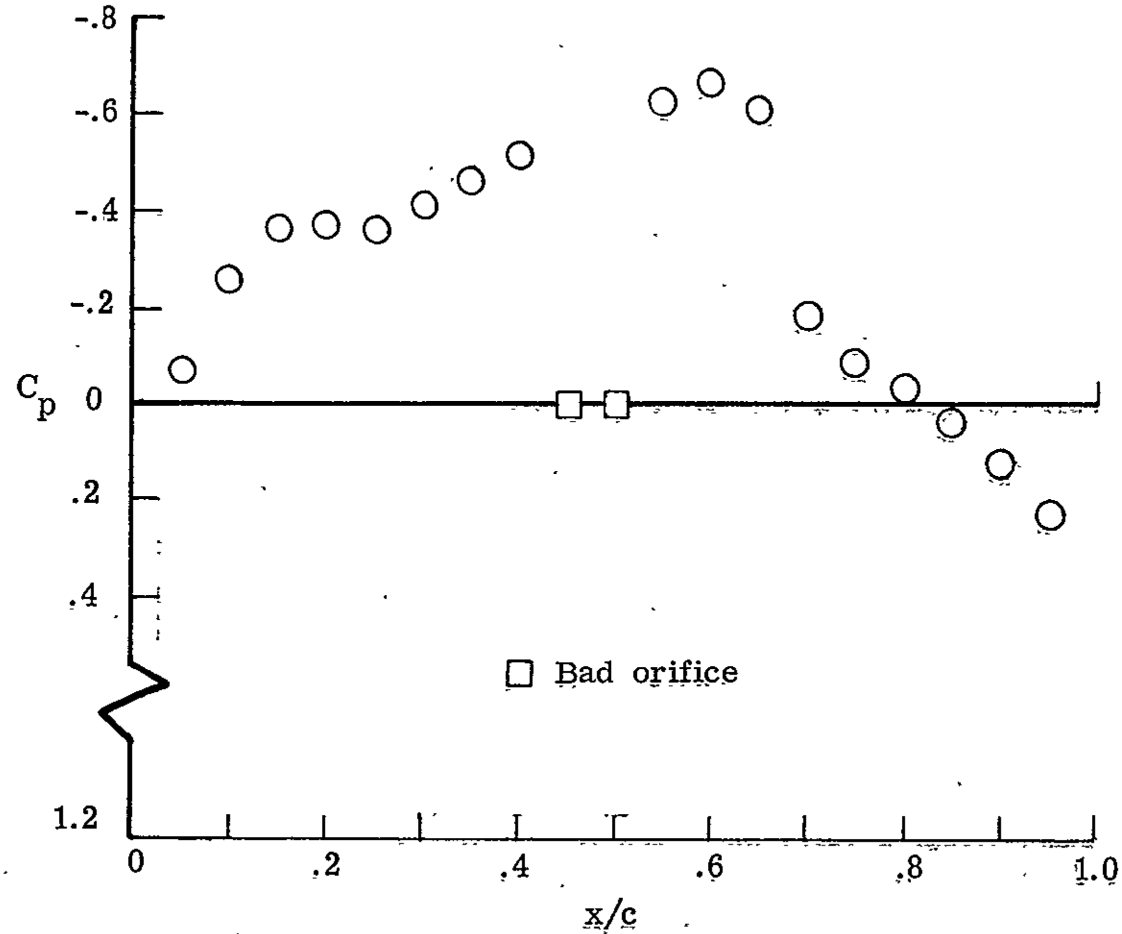

Figure 19.- Average unaffected pressure distribution for the $R_c = 42 \times 10^6$ path of the $M_\infty = 0.85$ test.

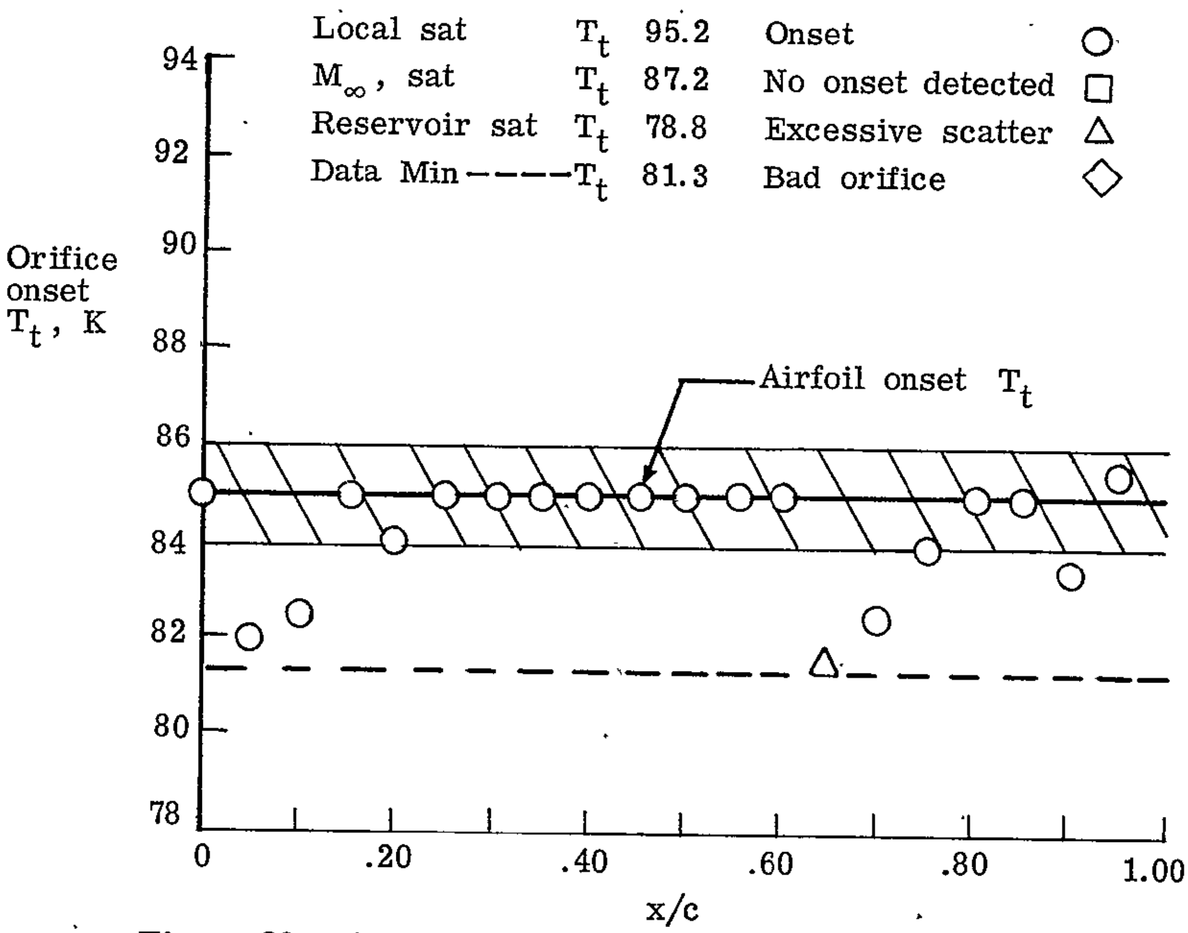

Figure 20.- Orifice onset T_t's and resulting airfoil onset T_t for the $R_c = 16 \times 10^6$ path of the $M_\infty = 0.85$ test.

ORIGINAL PAGE IS
OF POOR QUALITY

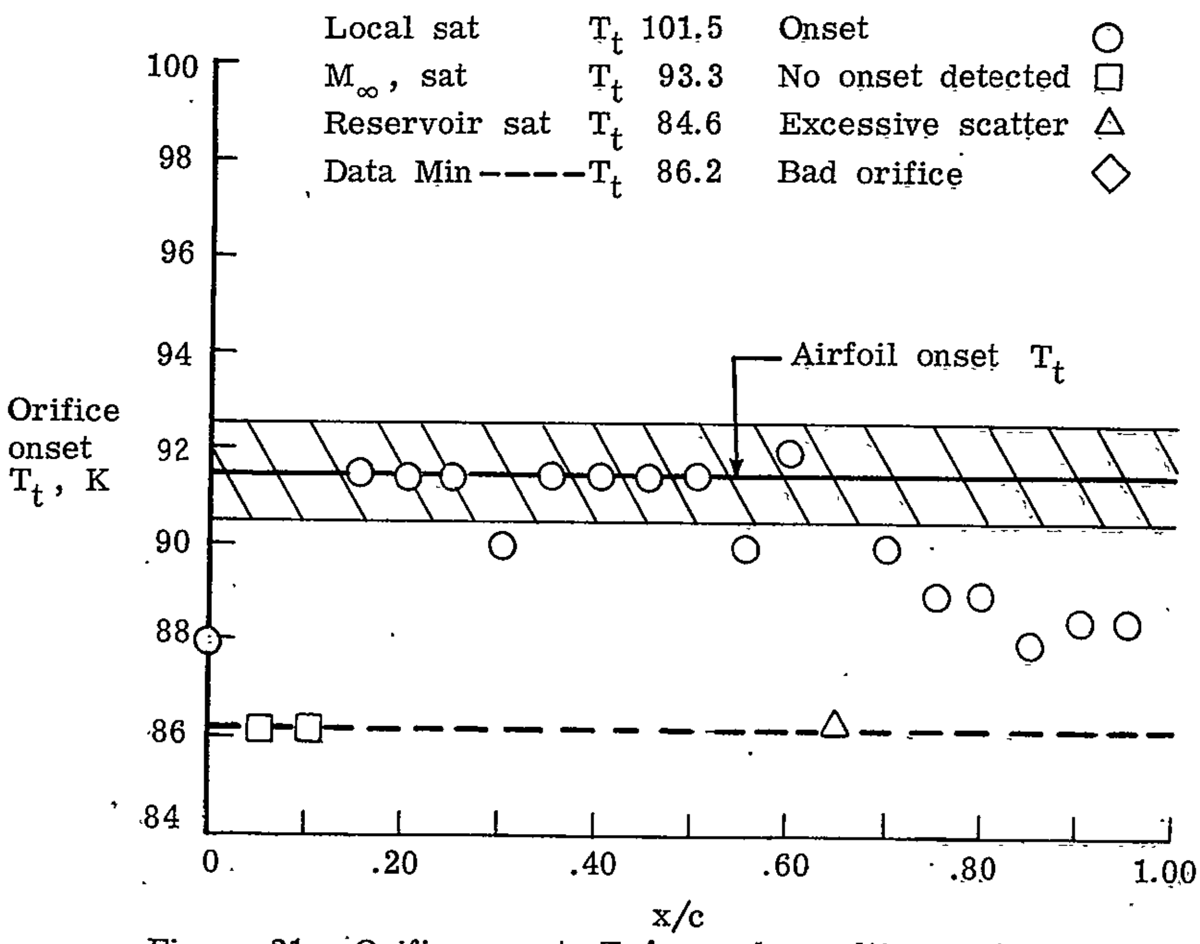

Figure 21.- Orifice onset T_t's and resulting airfoil onset T_t for the $R_c = 26 \times 10^6$ of the $M_\infty = 0.85$ test.

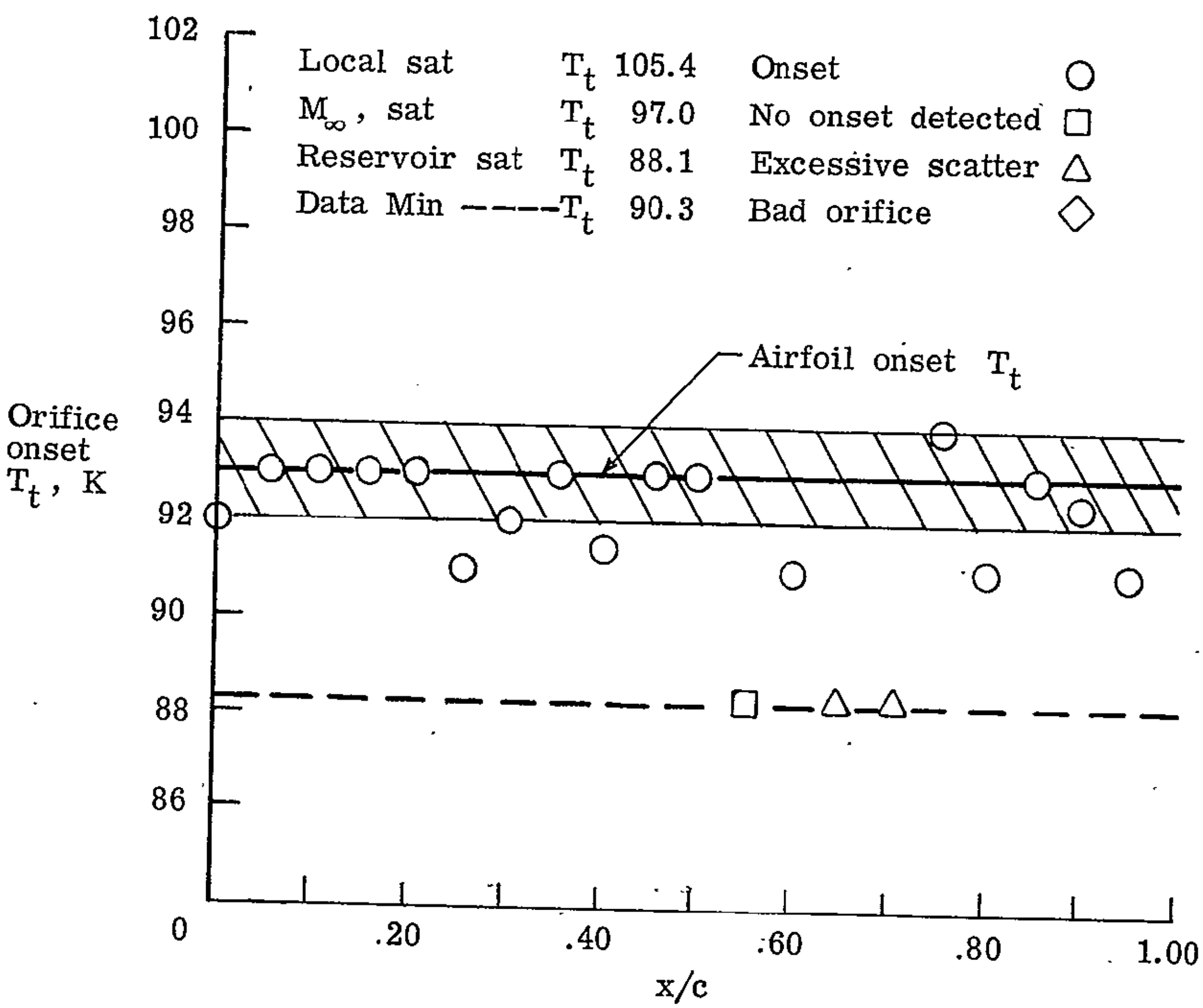

Figure 22.- Orifice onset T_t's and resulting airfoil onset T_t for the $R_c = 34 \times 10^6$ path of the $M_\infty = 0.85$ test.

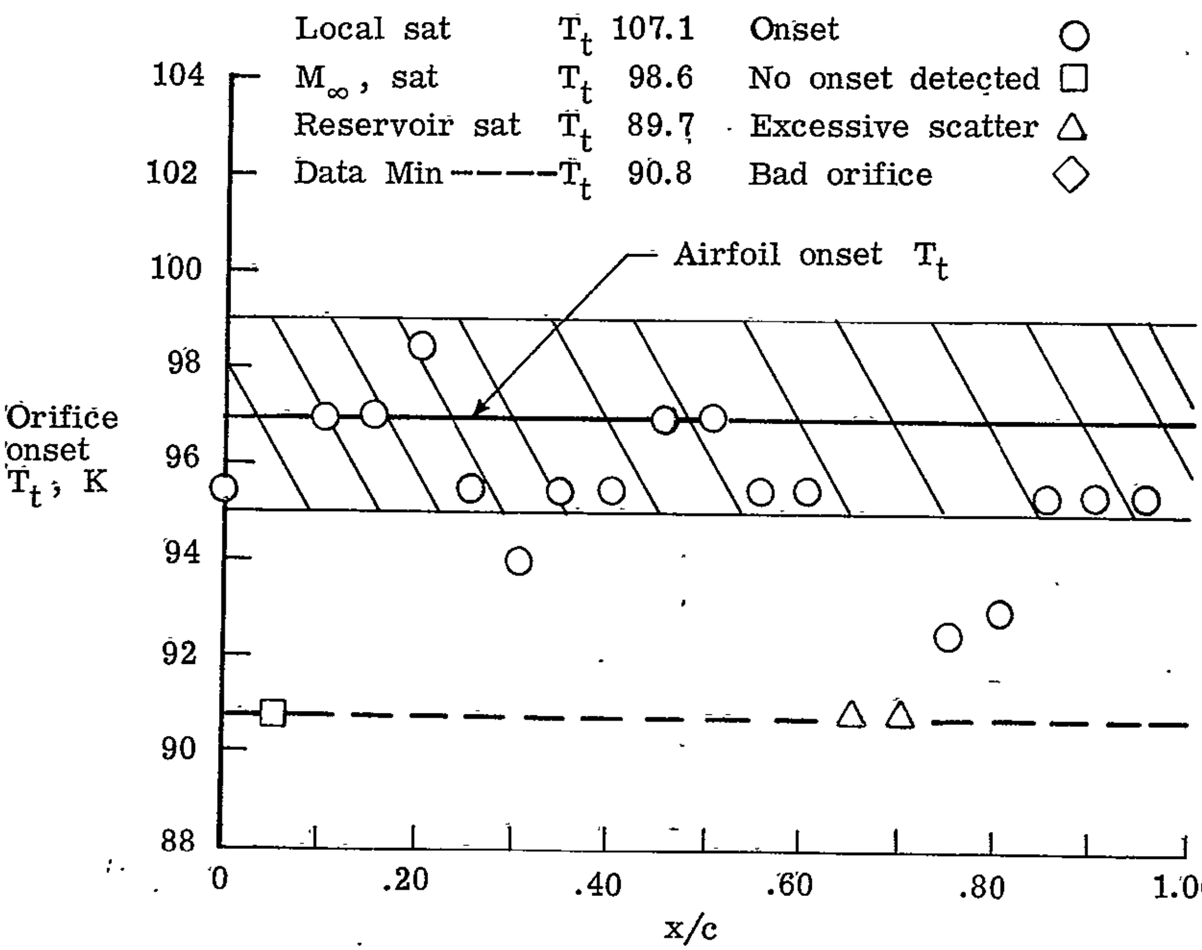

Figure 23.- Orifice onset T_t's and resulting airfoil onset T_t for the $R_c = 38 \times 10^6$ path of the $M_\infty = 0.85$ test.

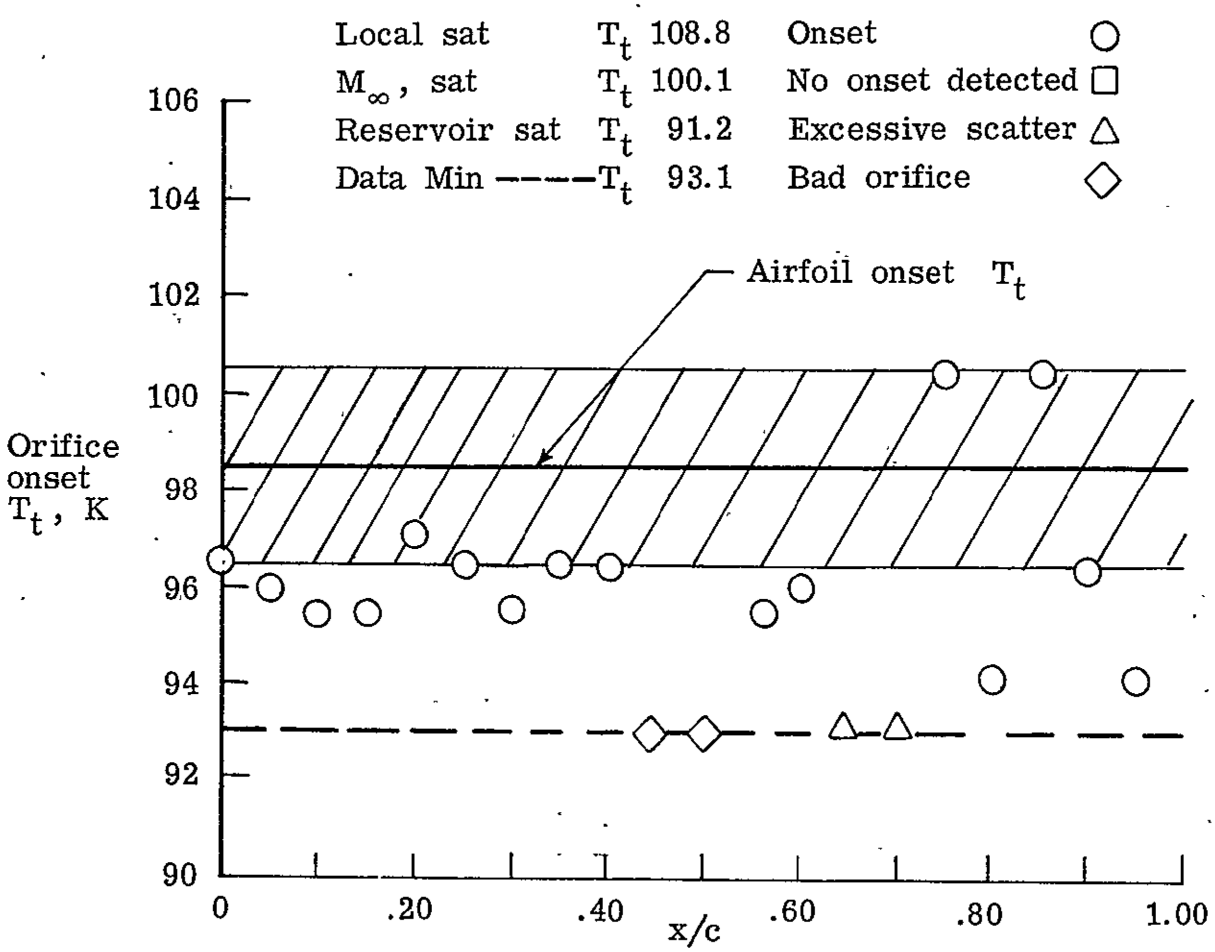

Figure 24.- Orifice onset T_t's and resulting airfoil onset T_t for the $R_c = 42 \times 10^6$ path of the $M_\infty = 0.85$ test.

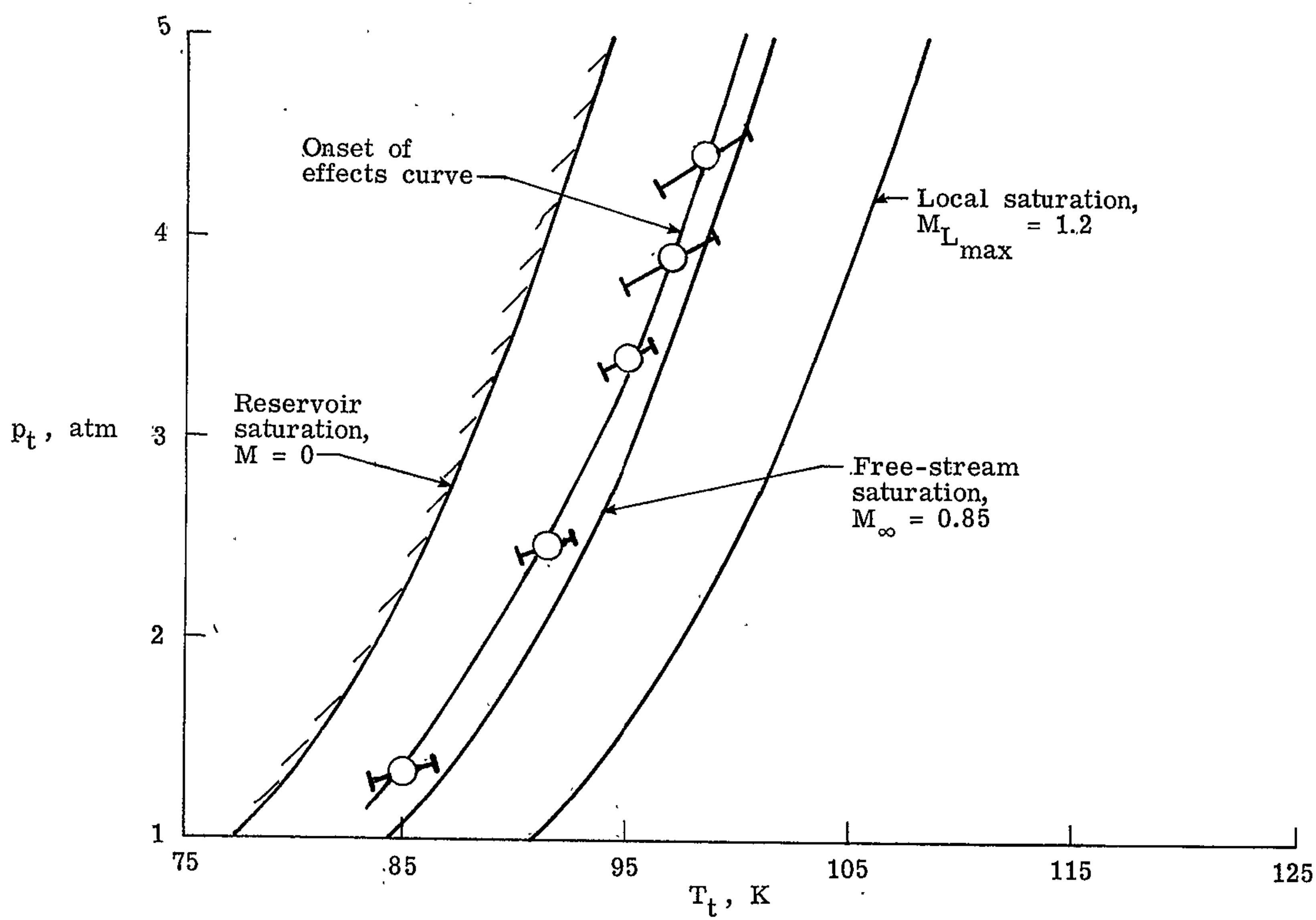

Figure 25.- Onset of condensation effects for $M_{\infty} = 0.85$ test.

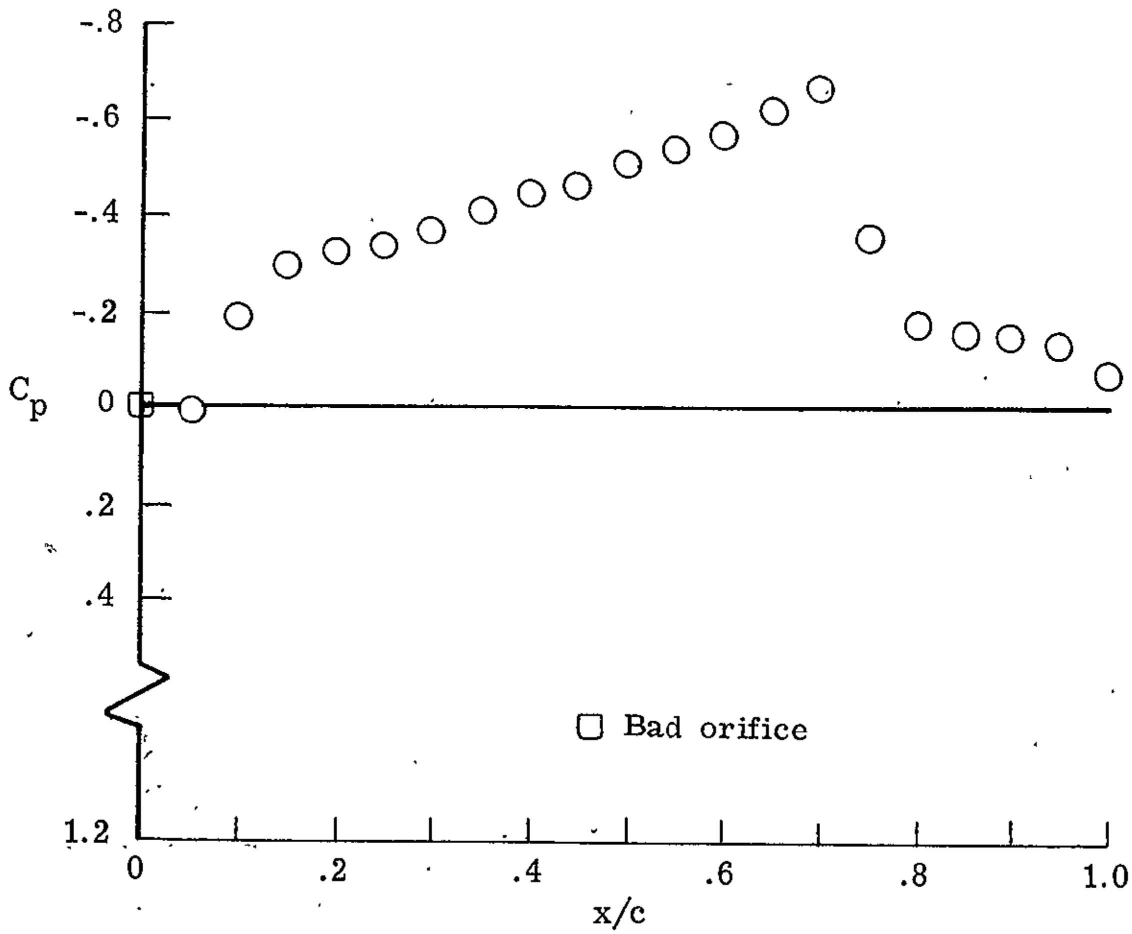

Figure 26.- Average unaffected pressure distribution for the $R_c = 16 \times 10^6$ path of the $M_\infty = 0.95$ test.

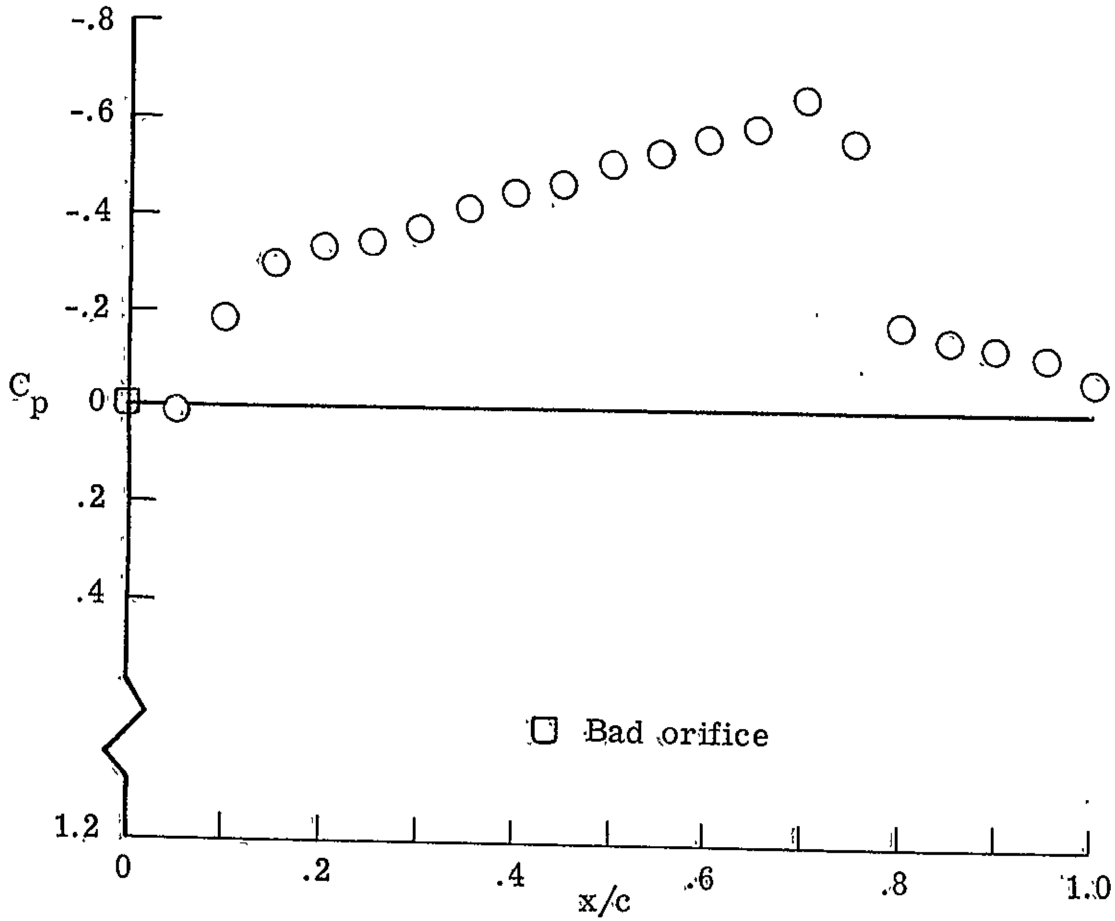

Figure 27.- Average unaffected pressure distribution for the $R_c = 27 \times 10^6$ path of the $M_\infty = 0.95$ test.

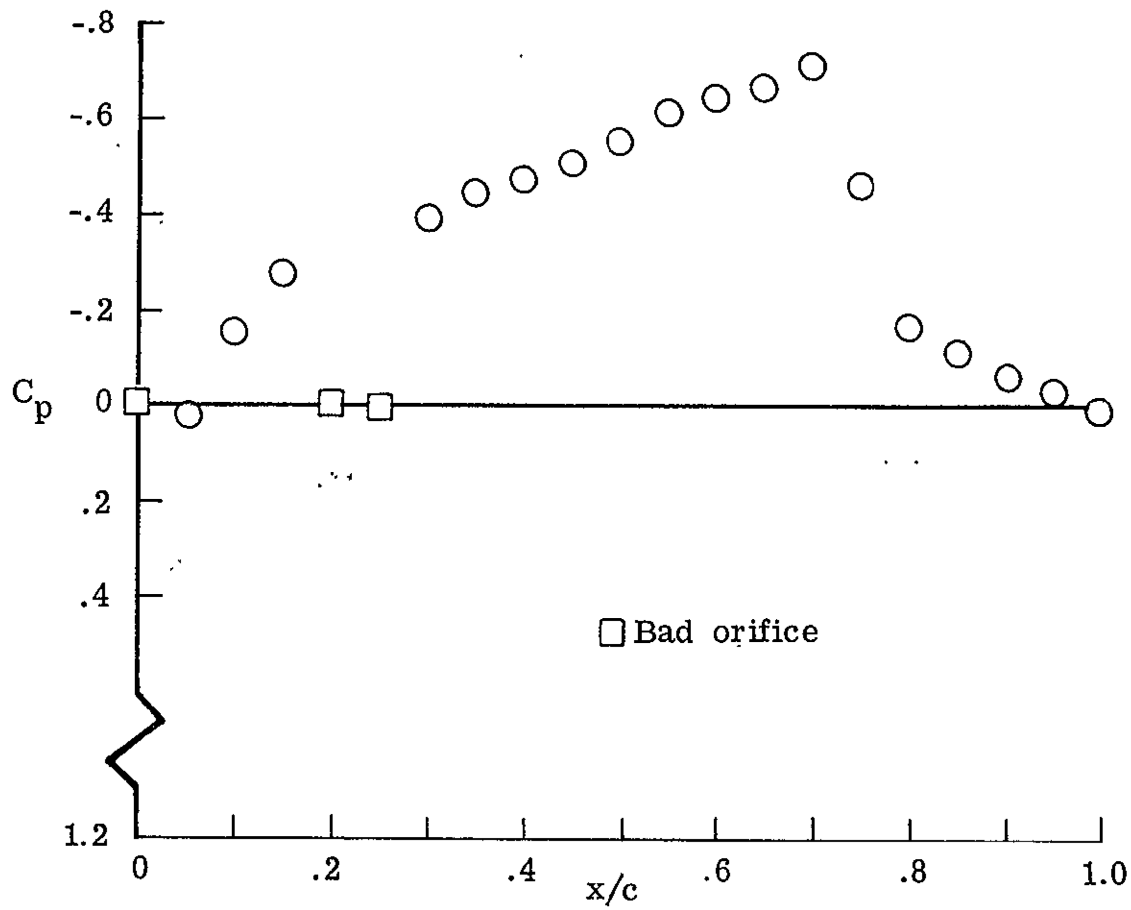

Figure 28.- Average unaffected pressure distribution for the $R_c = 40 \times 10^6$ path of the $M_\infty = 0.95$ test. ($M_\infty = 0.93$ for this path.)

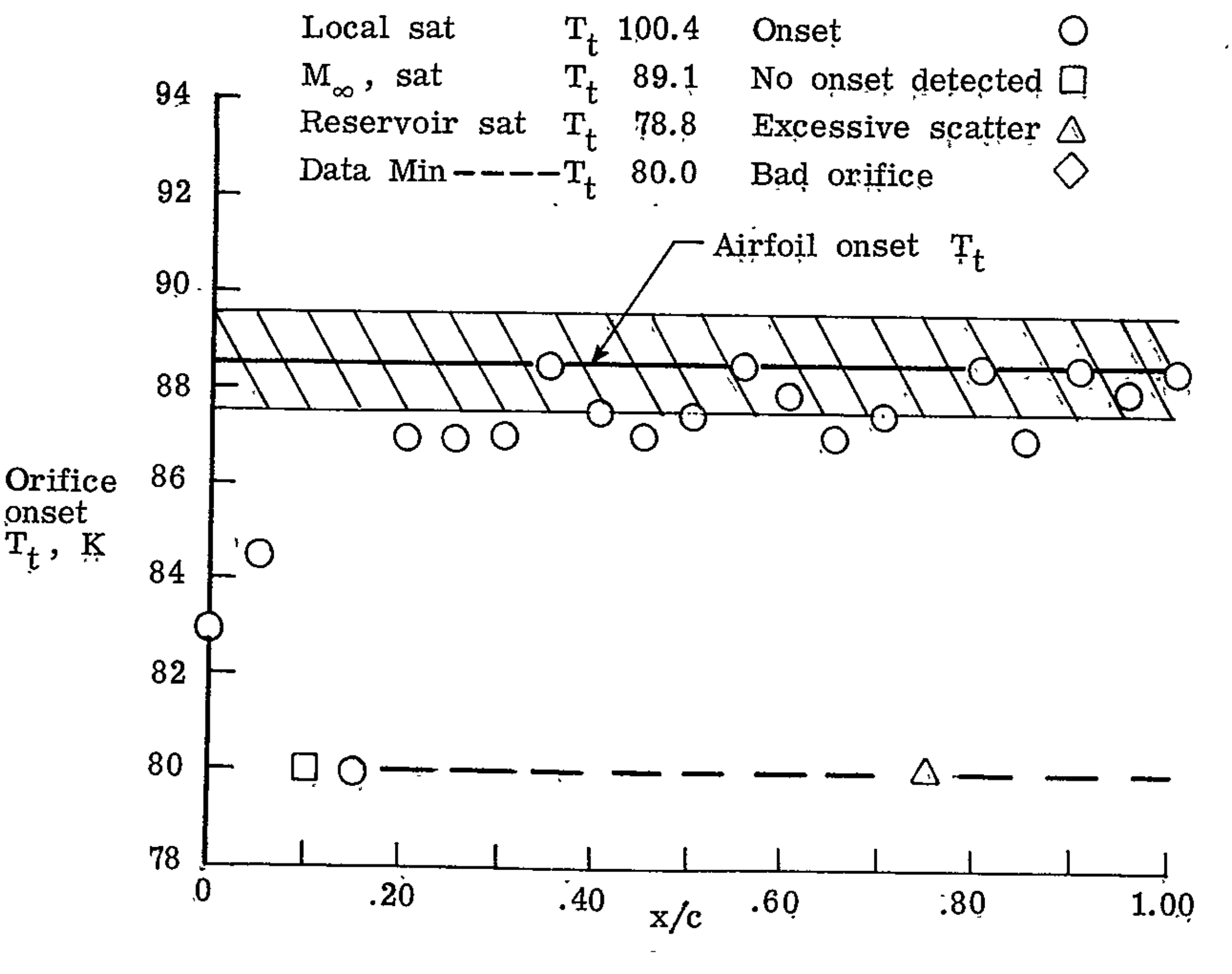

Figure 29.- Orifice onset T_t's and resulting airfoil onset T_t for the $R_c = 16 \times 10^6$ path of the $M_\infty = 0.95$ test.

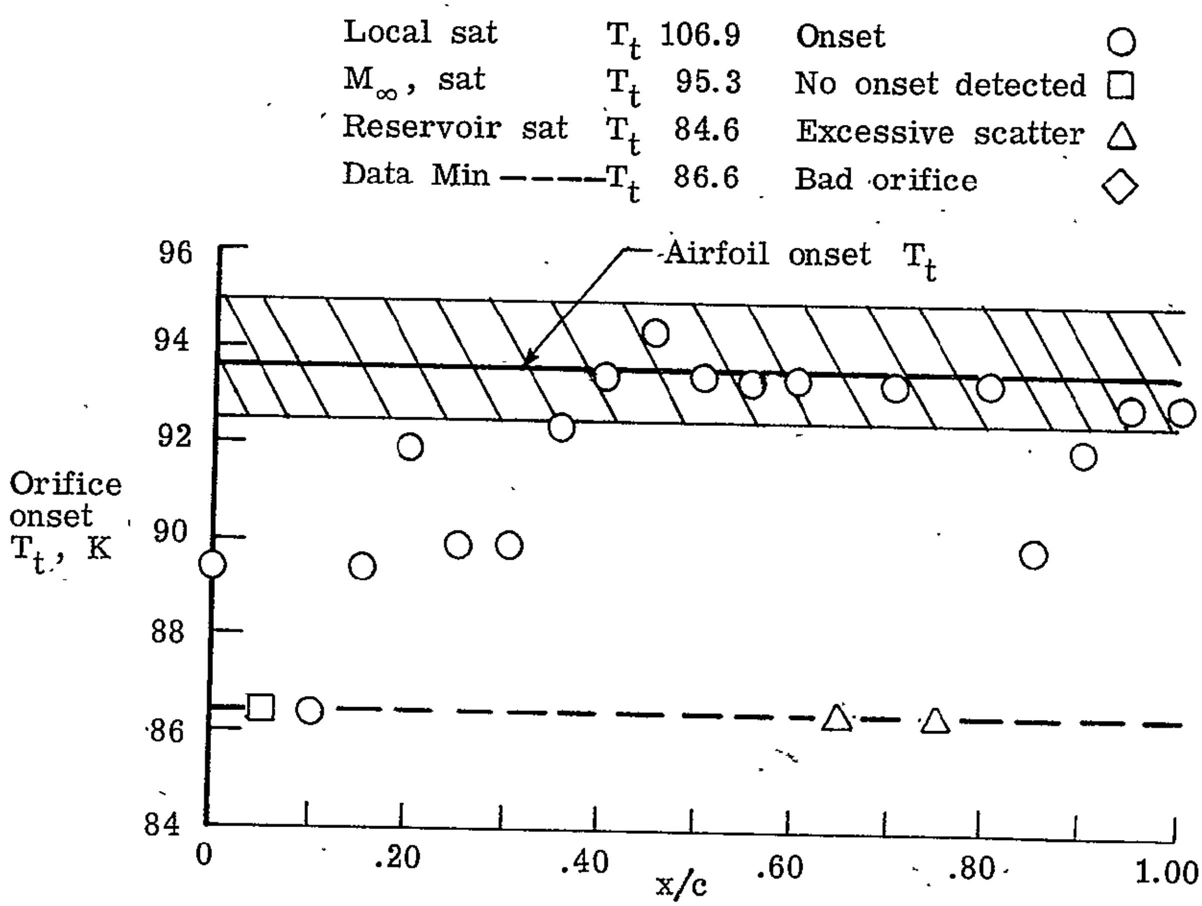

Figure 30.- Orifice onset T_t's and resulting airfoil onset T_t for the $R_c = 27 \times 10^6$ path of the $M_\infty = 0.95$ test.

ORIGINAL PAGE IS
OF POOR QUALITY

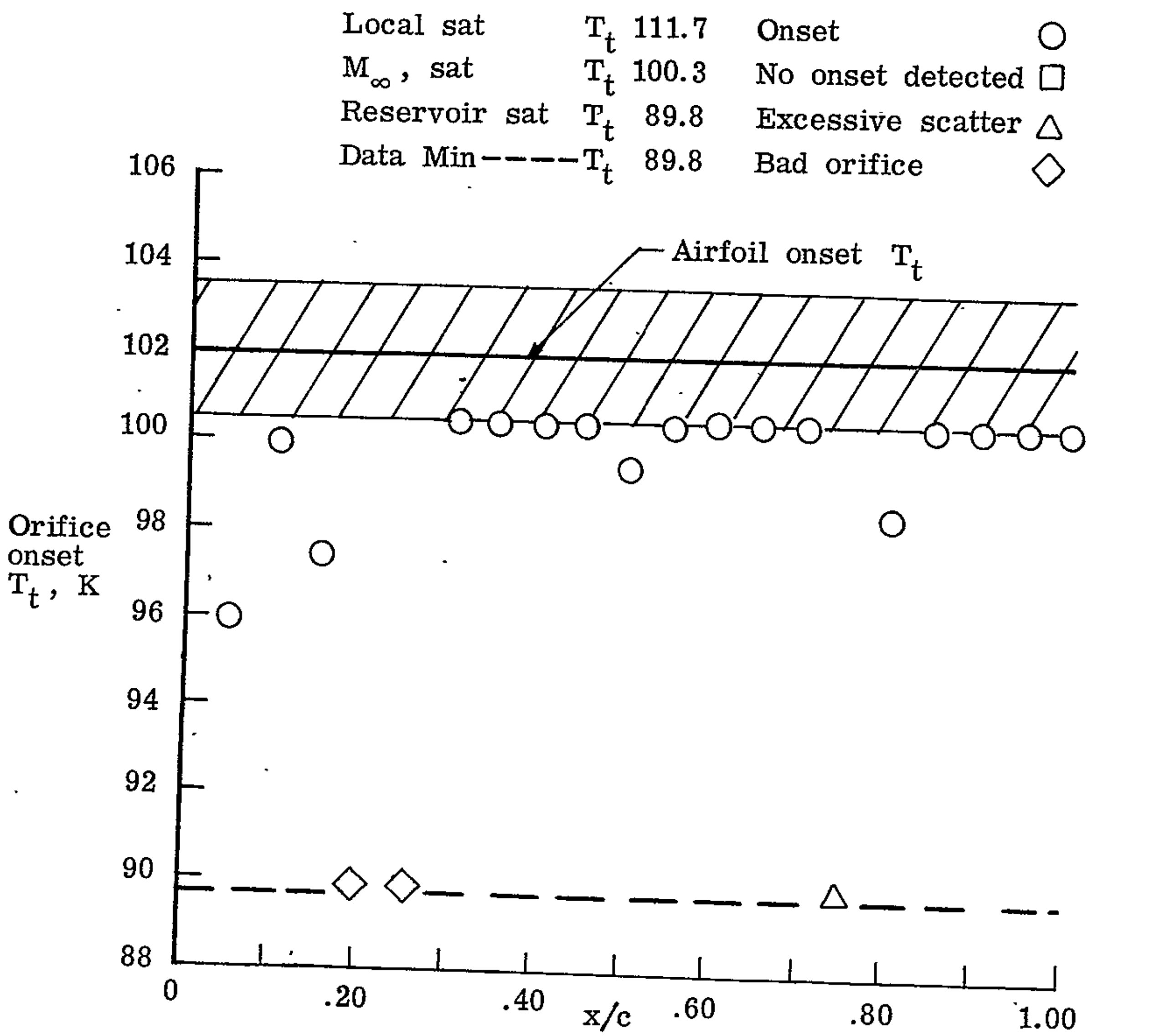

Figure 31.- Orifice onset T_t's and resulting airfoil onset T_t for the $R_c = 40 \times 10^6$ path of the $M_\infty = 0.95$ test.

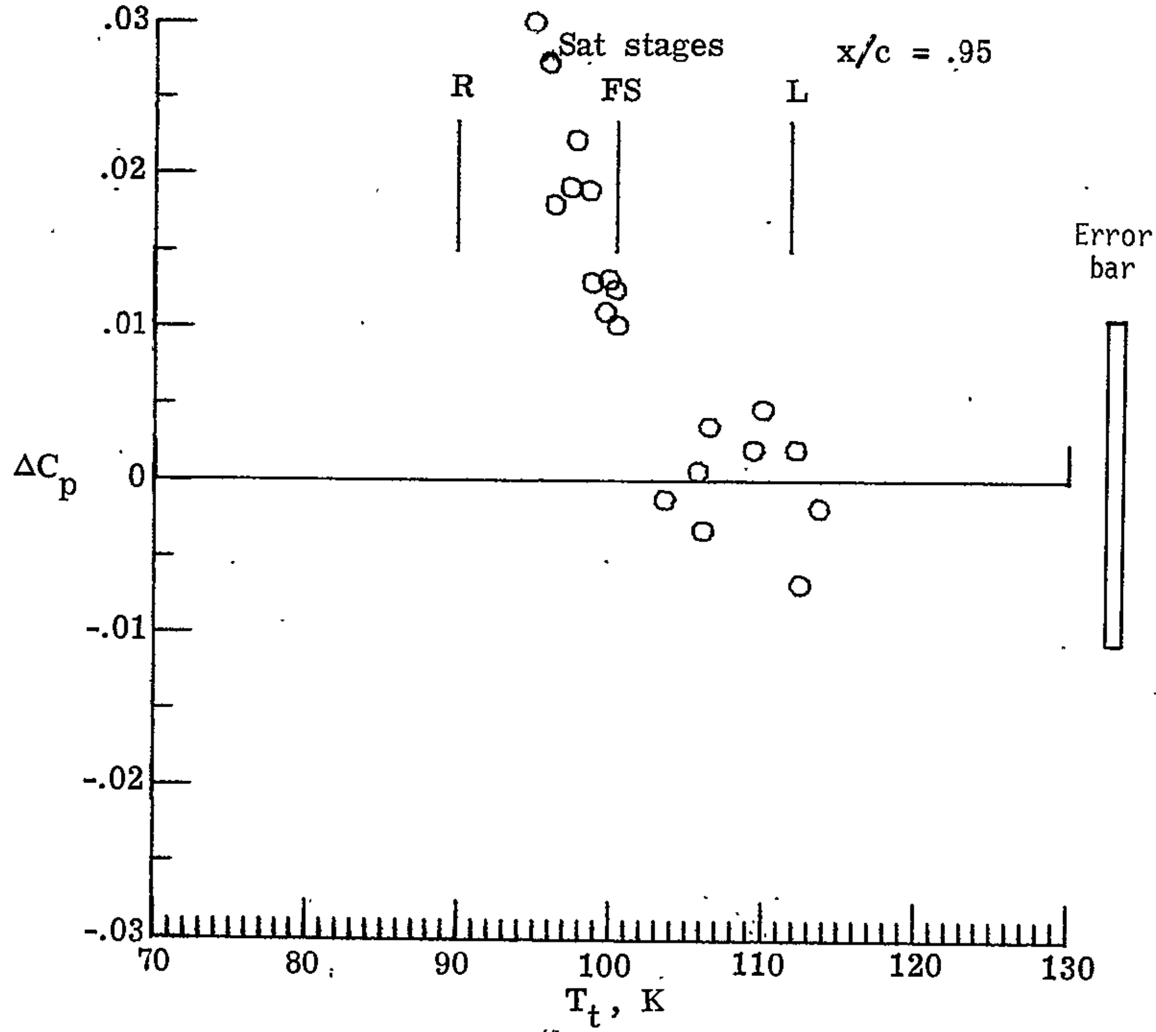

Figure 32.- ΔC_p vs. T_t for $M_\infty = 0.93$ and $R_c = 39.8$ million. Unaffected average value of $C_p = -0.035$.

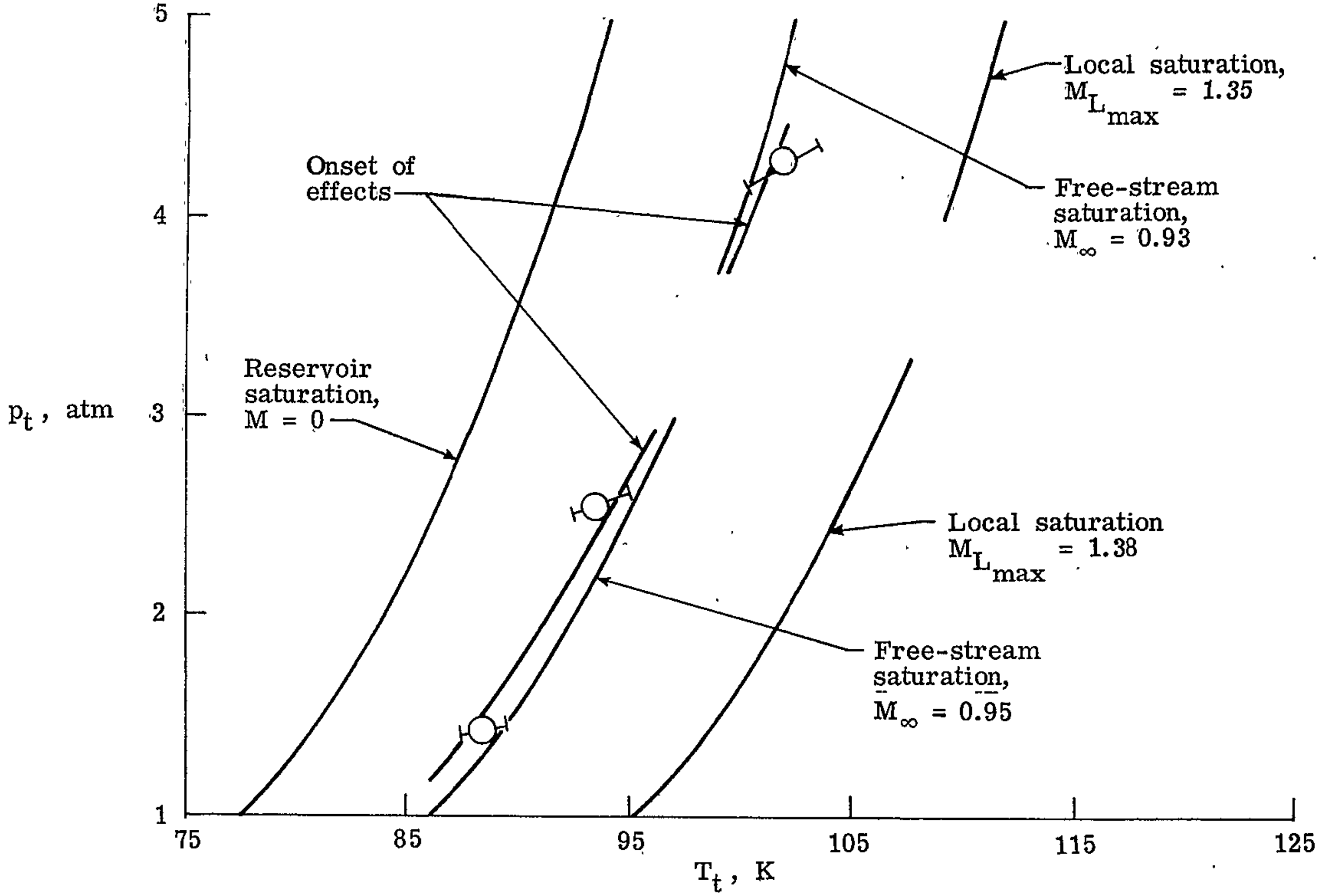

Figure 33.- Onset of condensation effects for the $M_\infty = 0.95$ test.

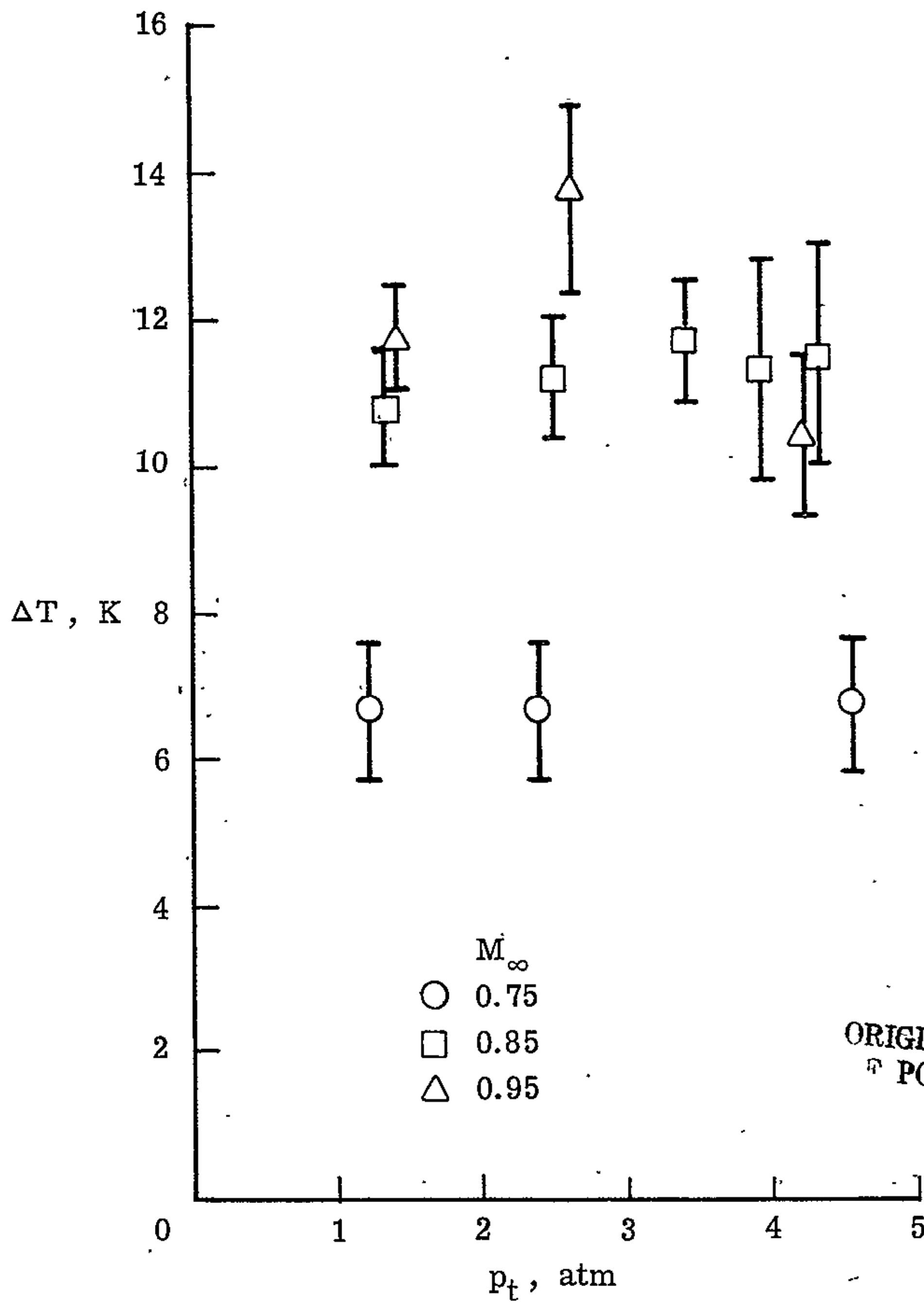

(a) Supercooling based on $M_{L_{max}}$

Figure 34.- Supercooling for all M_∞ tests.

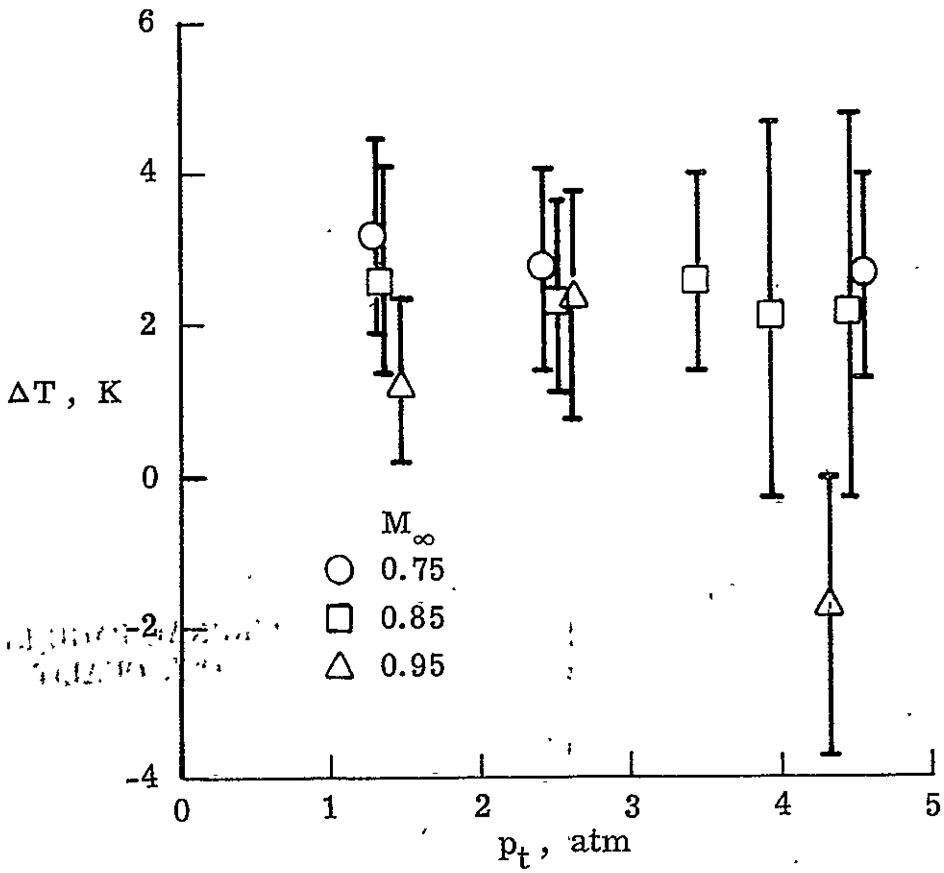

(b) Supercooling based on M_∞

Figure 34.- Concluded.

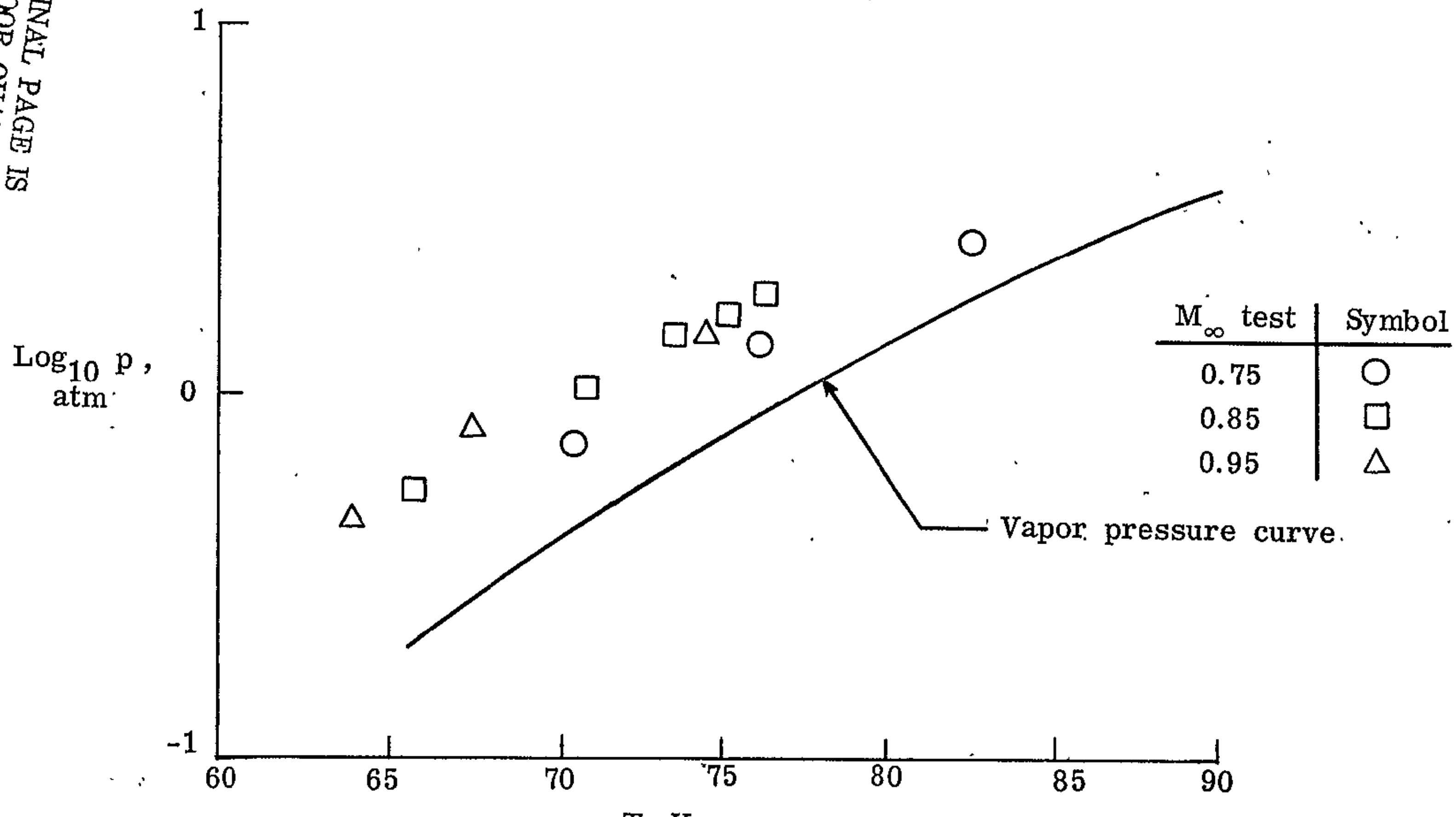

(a) Static values based on $M = M_{L_{max}}$

Figure 35.- Static values of p , T at onset.

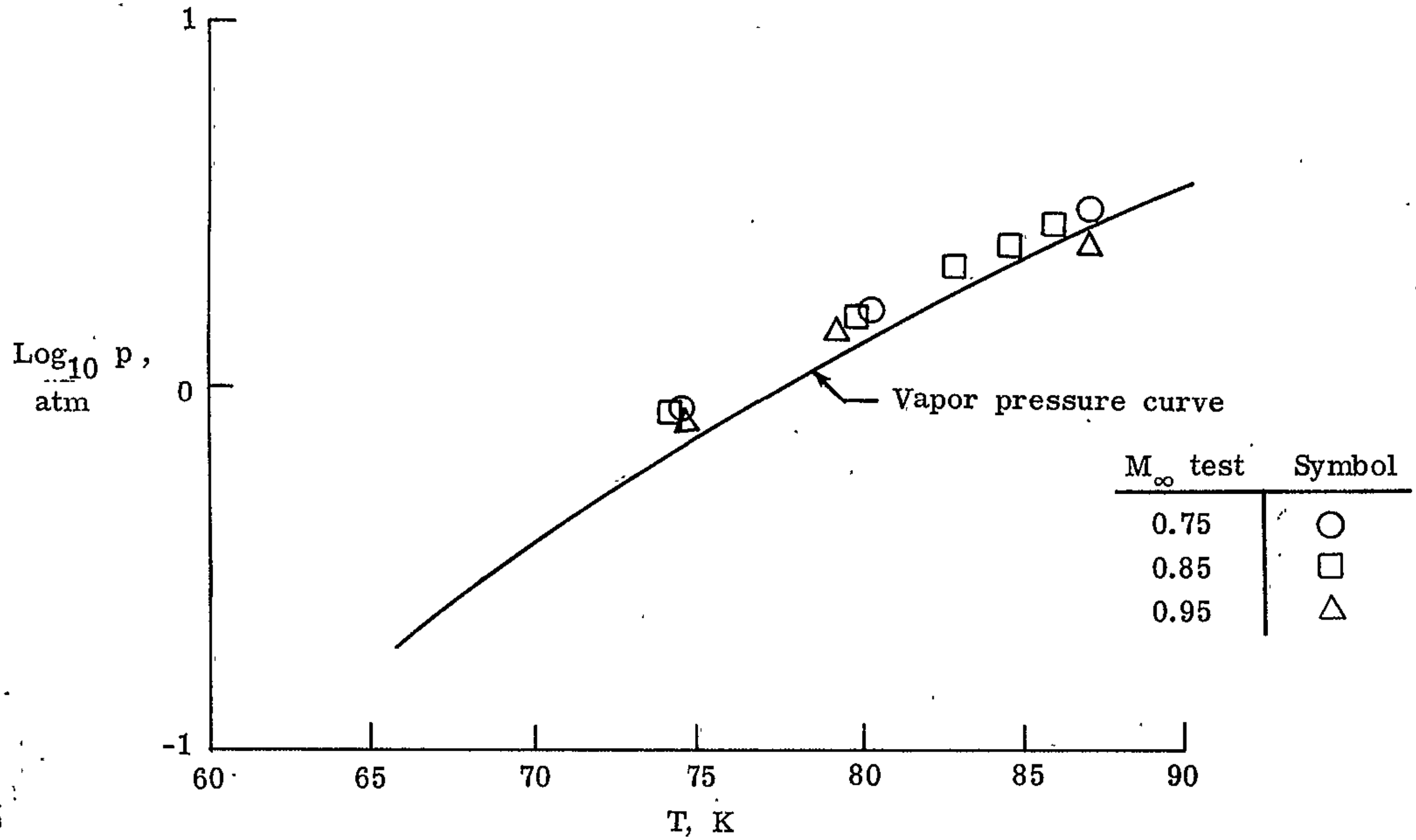

(b) Static values based on $M = M_\infty$.

Figure 35.- Concluded.

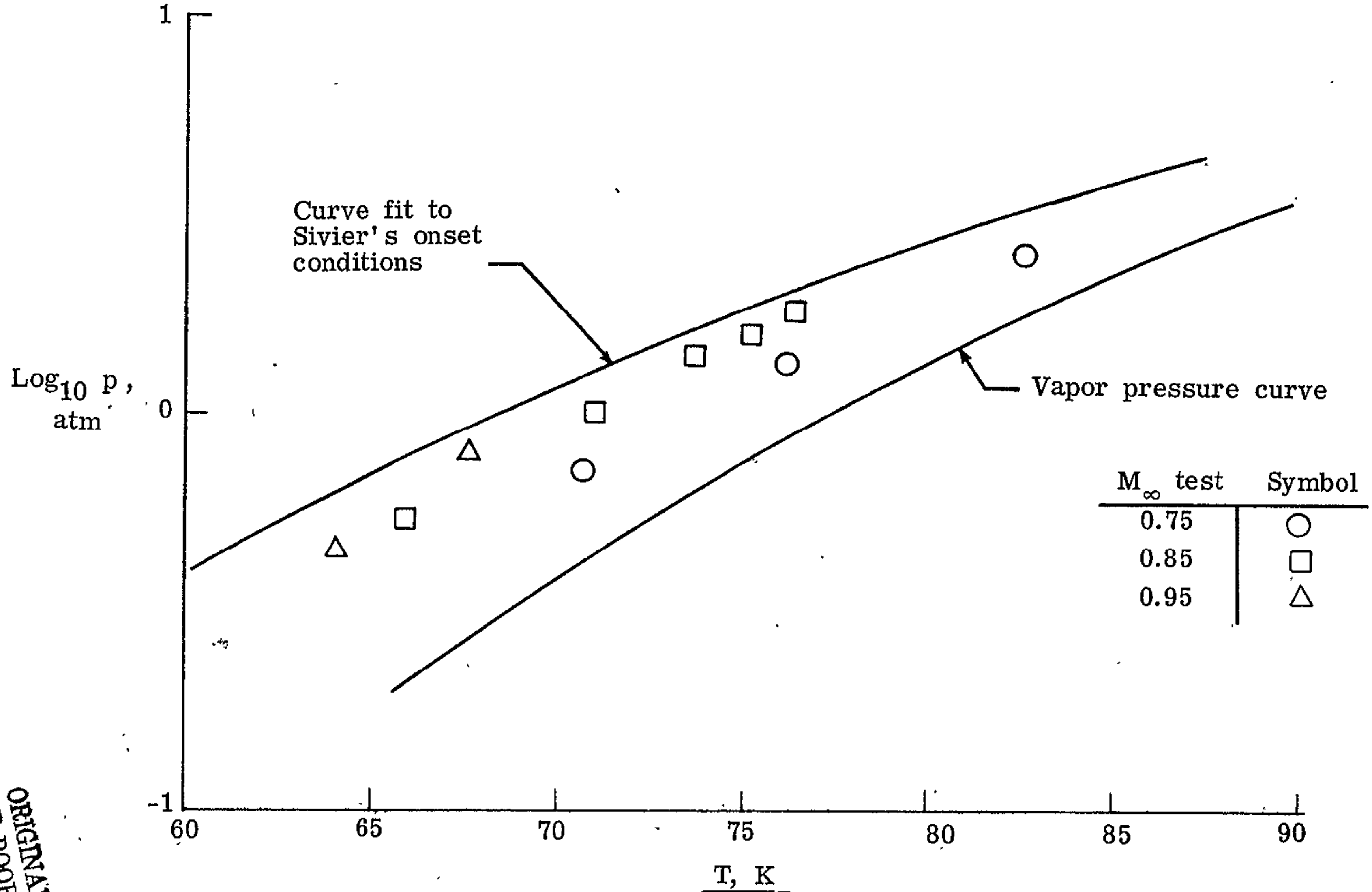

Figure 36.- Data compared with curve fit to Siver's analytically determined onset conditions.

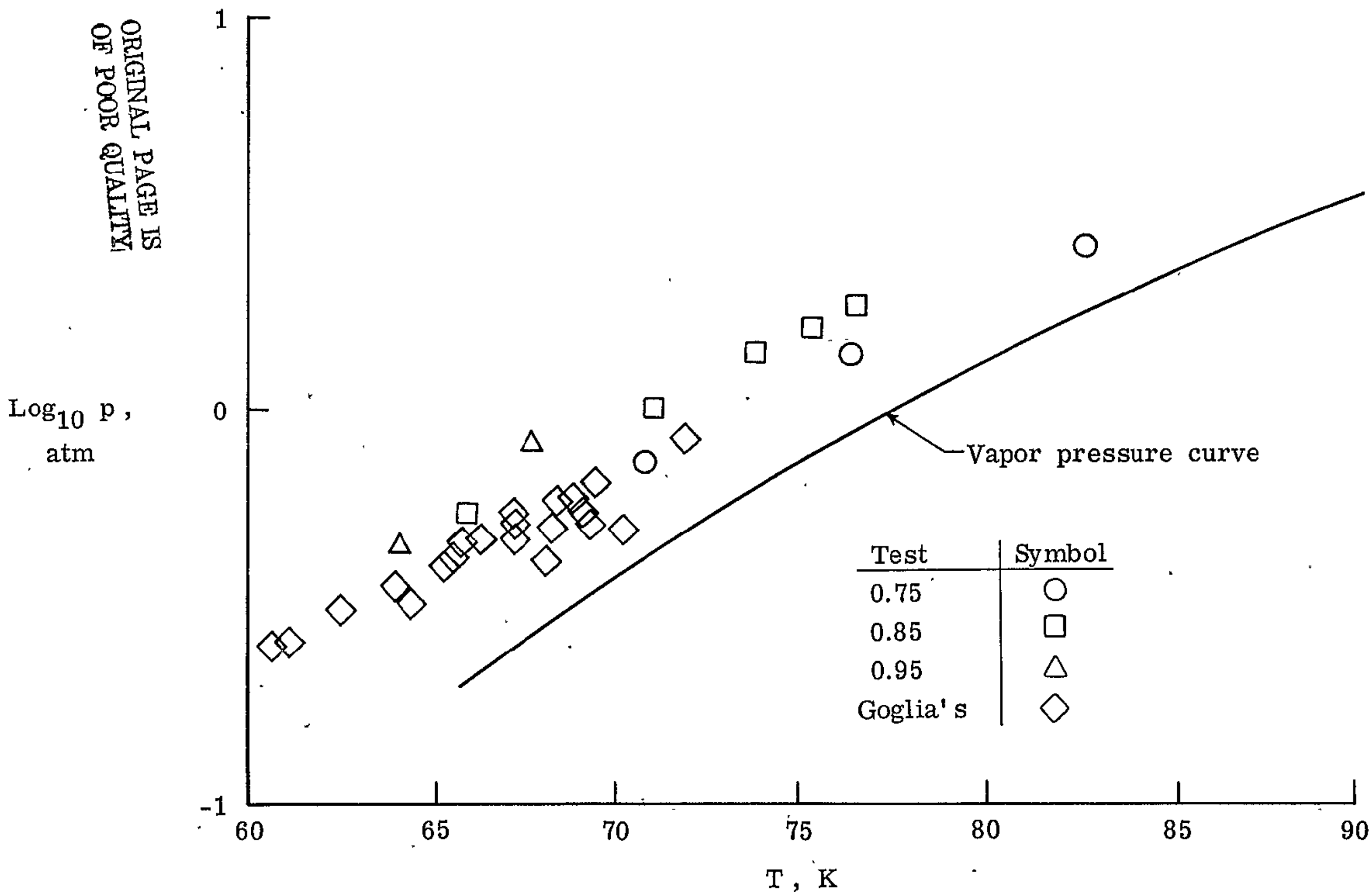

Figure 37.- Data compared to Goglia's data from reference 18.

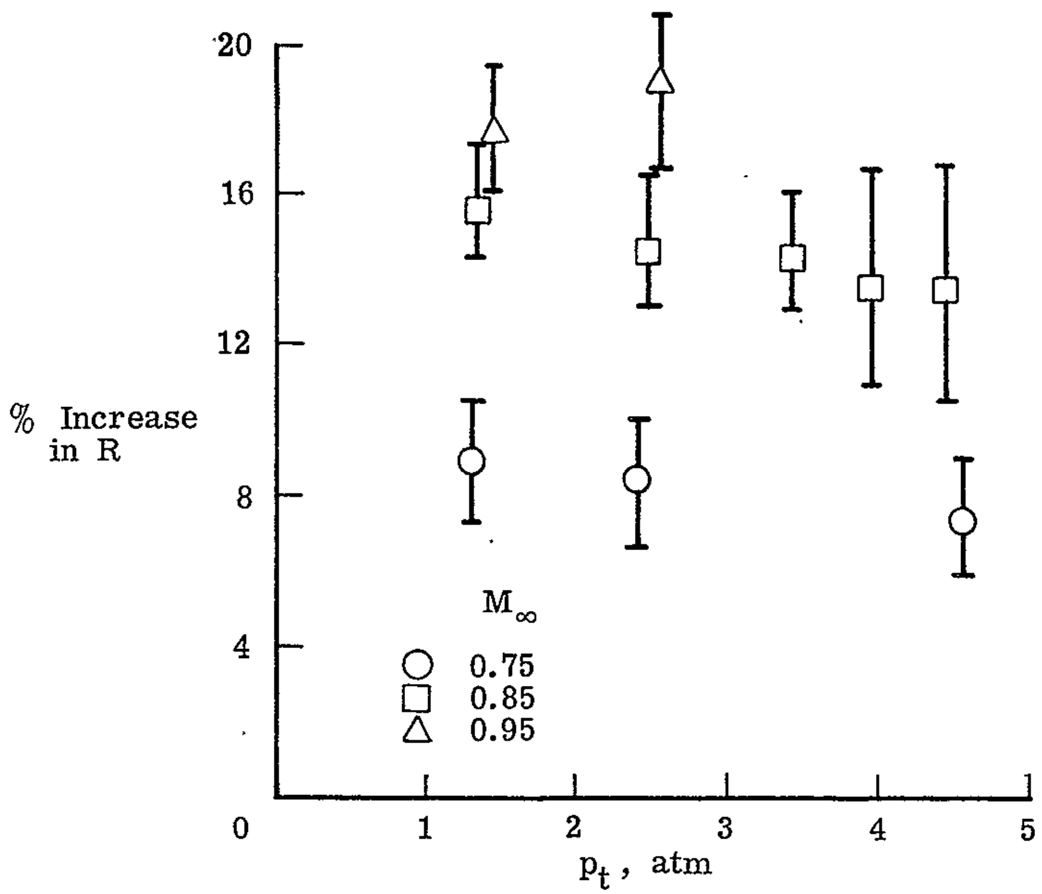

Figure 38.- Percent increase in Reynolds number capability at onset.

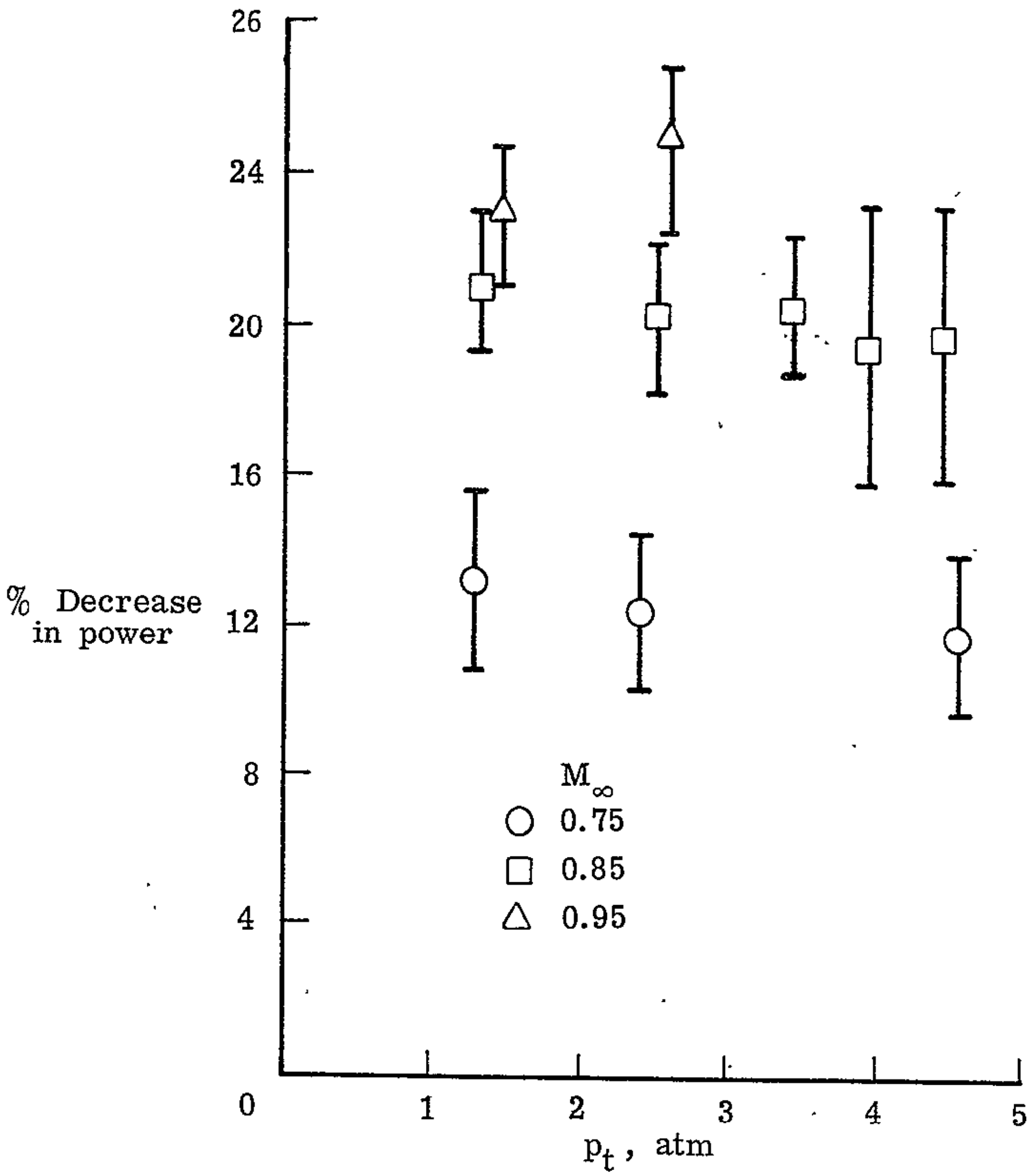

Figure 39.- Percent decrease in drive fan power at onset.

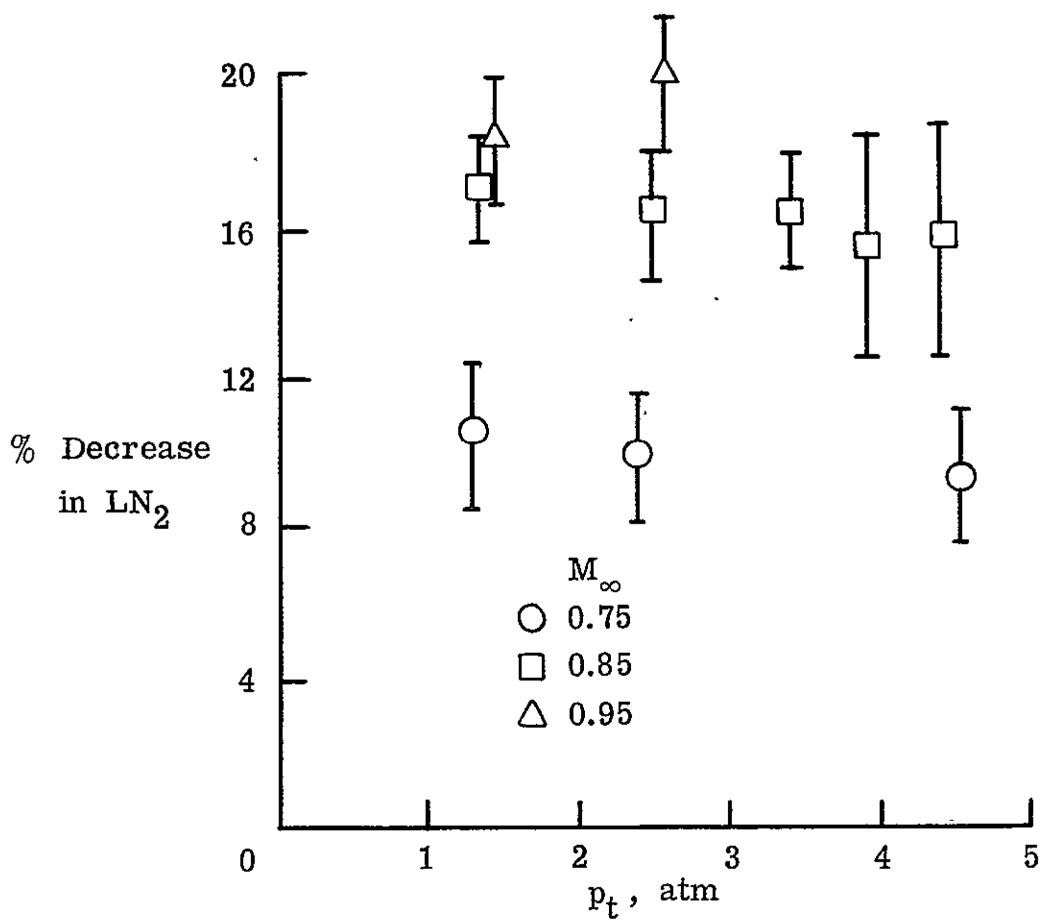

Figure 40.- Percent decrease in LN_2 required to absorb drive fan heat.

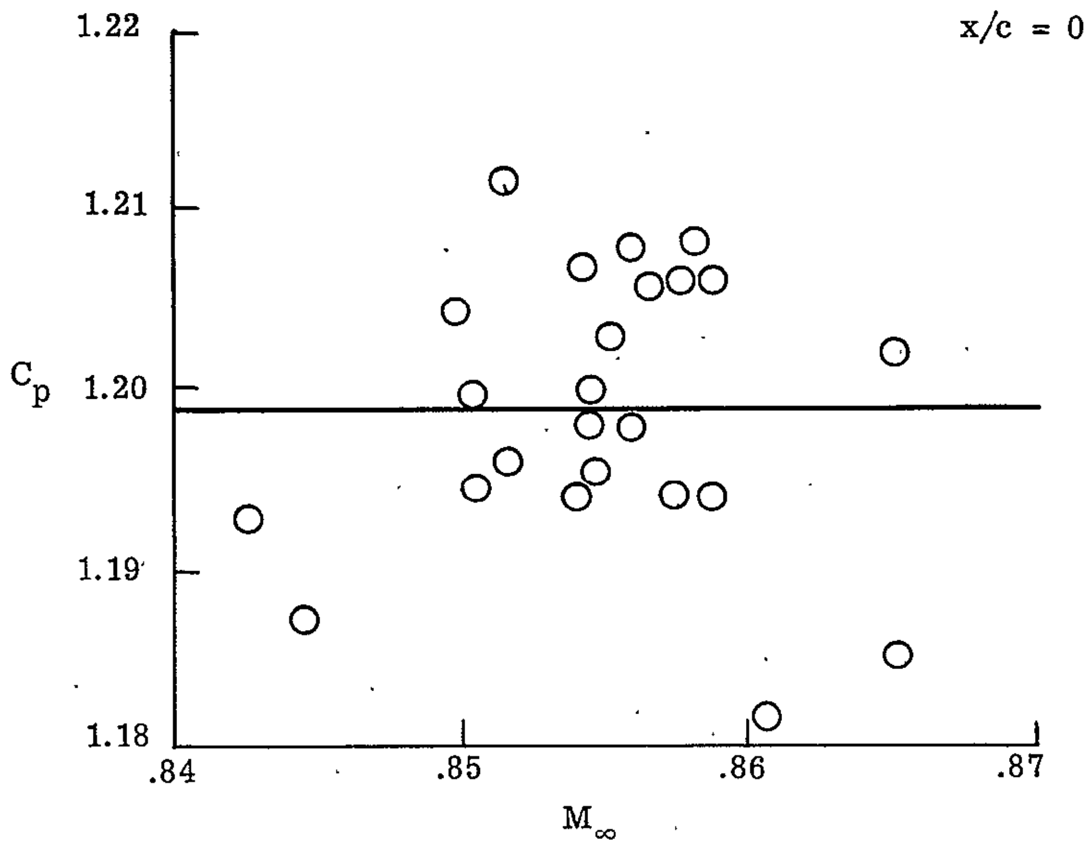

(a) r = 0.15.

Figure 41.- Examples of curve fits and resulting correlation coefficient, r.

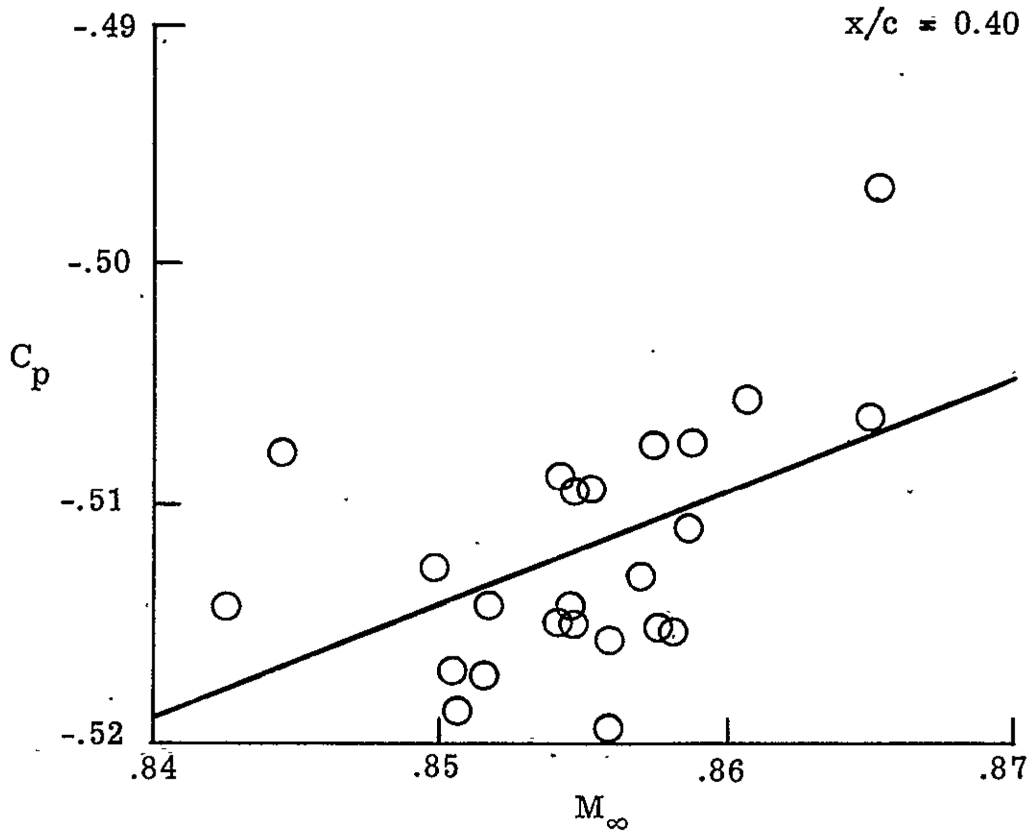

(b) r = 0.49.

Figure 41.- Continued.

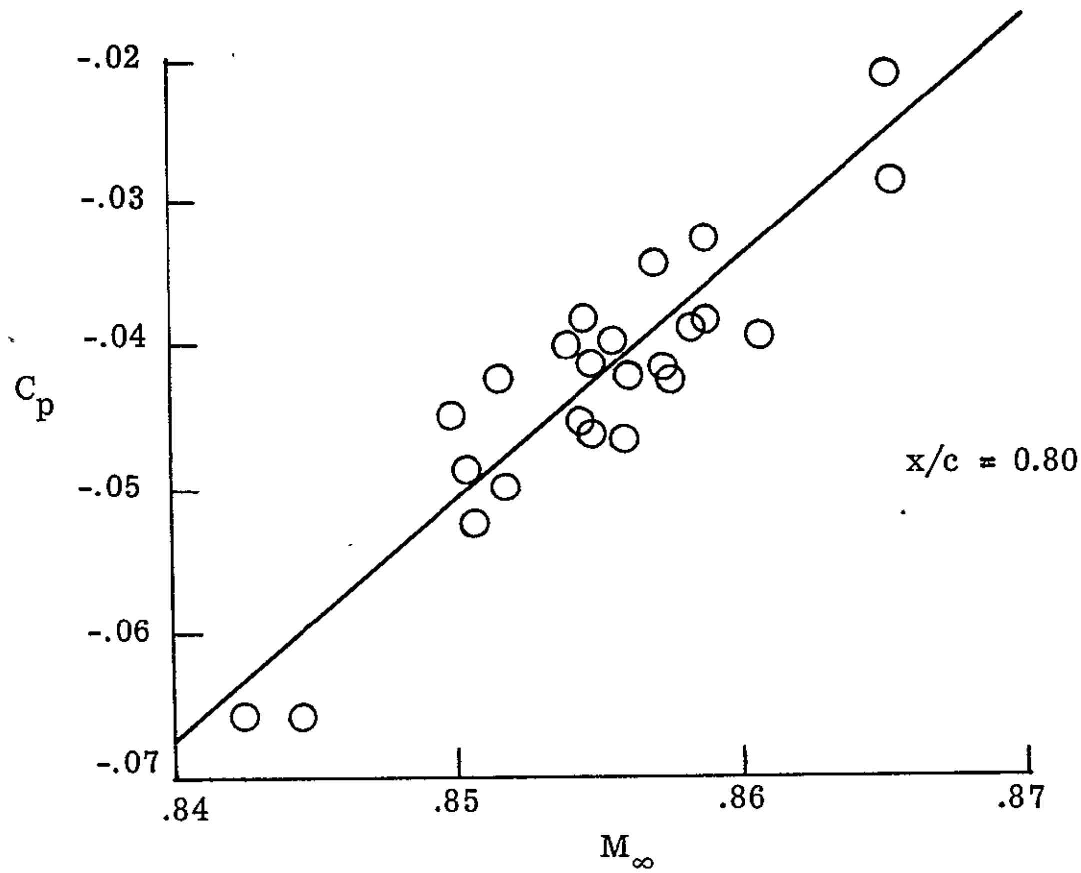

(c) r = 0.92.

Figure 41.- Concluded.

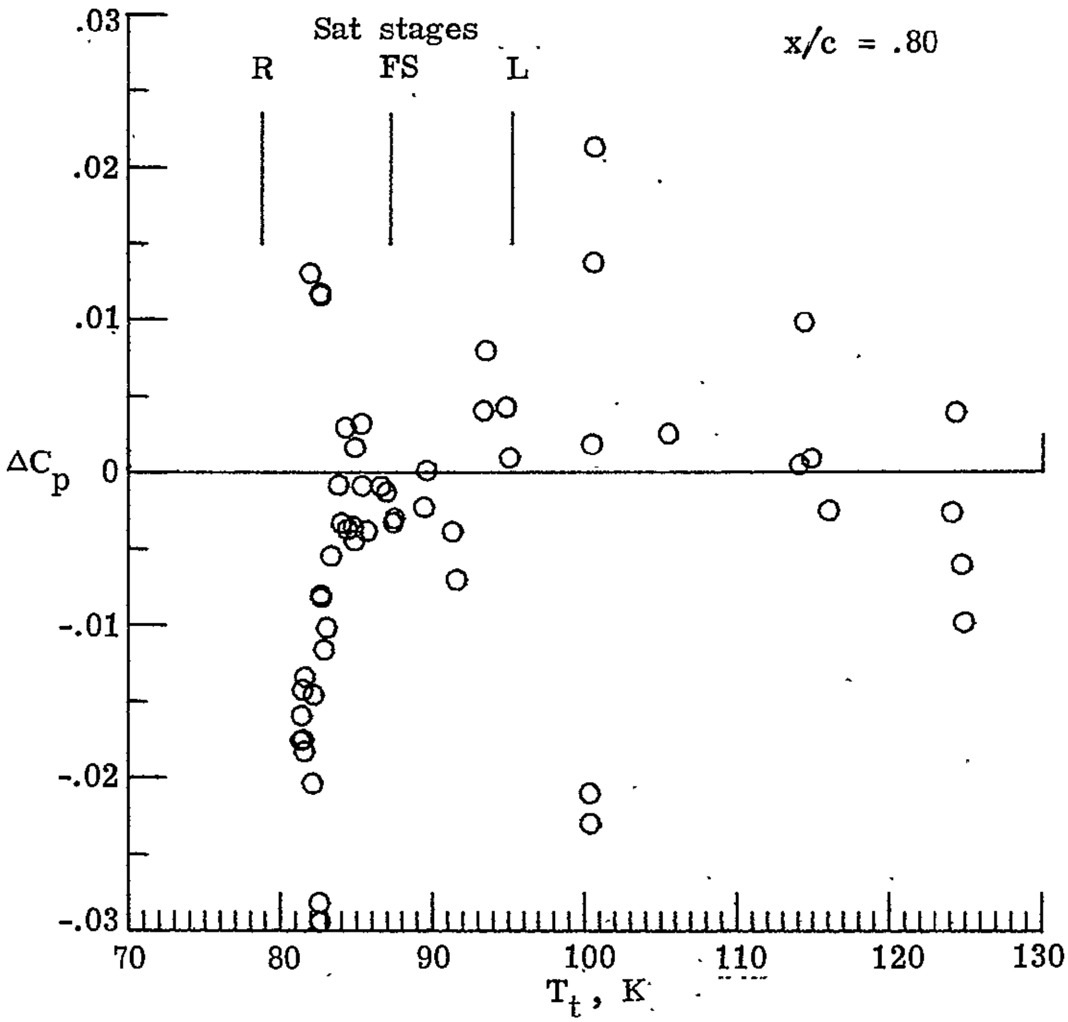

(a) Before Mach correction.

Figure 42.- Improvement in graphs of ΔCp vs. T_t with Mach correction for M_∞ = 0.85 and R_c = 16 million. Unaffected average value of Cp = -0.042.

ORIGINAL PAGE IS
OF POOR QUALITY

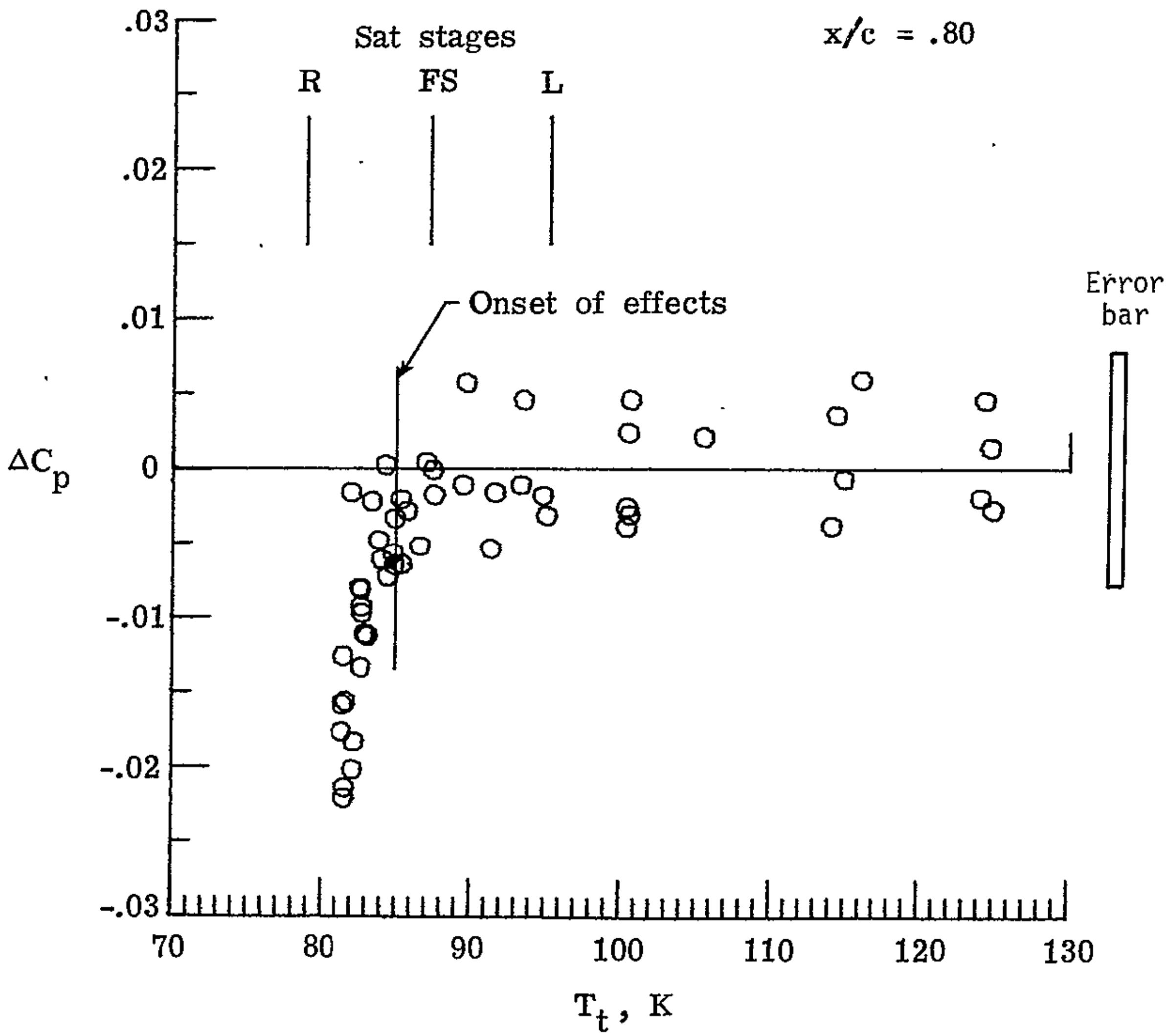

(b) After Mach correction.

Figure 42.- Concluded.

1. Report No. NASA TM 78666	2. Government Accession No.	3. Recipient's Catalog No.
4. Title and Subtitle ONSET OF CONDENSATION EFFECTS WITH A NACA 0012-64 AIRFOIL TESTED IN THE LANGLEY 0.3-METER CRYOGENIC TUNNEL		5. Report Date March 1978
		6. Performing Organization Code 3850
7. Author(s) Robert M. Hall		8. Performing Organization Report No.
		10. Work Unit No.
9. Performing Organization Name and Address NASA Langley Research Center Hampton, Virginia 23665		11. Contract or Grant No.
		13. Type of Report and Period Covered Technical Memorandum
12. Sponsoring Agency Name and Address National Aeronautics and Space Administration Washington, DC 20546		14. Sponsoring Agency Code

15. Supplementary Notes

Material will be converted to a formal publication by January 1979.

16. Abstract

A 0.137-m NACA 0012-64 airfoil has been tested in the Langley 0.3-m transonic cryogenic tunnel at free-stream Mach numbers of 0.75, 0.85, and 0.95 over a total pressure range from 1.2 to 5.0 atmospheres. The onset of condensation effects were found to correlate more with the amount of supercooling in the free-stream than it did with the supercooling in the region of maximum local Mach number over the airfoil. Effects in the pressure distribution over the airfoil were generally seen to appear over its entire length at nearly the same total temperature. Both observations suggest the possibility of heterogeneous nucleation occurring in the free-stream. Comparisons of the present onset results are made to calculations by Sivier and data by Goglia. The potential operational benefits of the supercooling realized are then presented in terms of increased Reynolds number capability at a given tunnel total pressure, reduced drive fan power if Reynolds number is held constant, and reduced liquid nitrogen consumption if Reynolds number is again constant. Depending on total pressure and free-stream Mach number, these three benefits are found to,respectively, vary from 7 to 19 percent, 11 to 25 percent, and 9 to 20 percent.

17. Key Words (Suggested by Author(s))	18. Distribution Statement
Cryogenic Wind Tunnels Condensation Supercooling	Unclassified - Unlimited Star Category - 02

19. Security Classif. (of this report)	20. Security Classif. (of this page)	21. No. of Pages	22. Price*
Unclassified	Unclassified	84	$5.00

* For sale by the National Technical Information Service, Springfield, Virginia 22161